The Downward Influence of Sudden Stratospheric Warmings: Association with Tropospheric Precursors

Ian White*

The Hebrew University of Jerusalem, Institute of Earth Sciences, Edmond J. Safra Campus, Givat Ram, Jerusalem, Israel

Chaim I. Garfinkel

The Hebrew University of Jerusalem, Institute of Earth Sciences, Edmond J. Safra Campus, Givat Ram, Jerusalem, Israel

Edwin P. Gerber

Courant Institute of Mathematical Sciences, New York University, New York, USA

Martin Jucker

School of Earth Sciences, The University of Melbourne, Parkville, Australia

Valentina Aquila

American University, Dept of Environmental Science, Washington, DC, USA

Luke D. Oman

NASA Goddard Space Flight Center, Greenbelt, Maryland, USA

*Corresponding author address: Ian White, The Hebrew University of Jerusalem, Institute of Earth Sciences, Edmond J. Safra Campus, Givat Ram, Jerusalem, Israel.
E-mail: ian.white@mail.huji.ac.il

ABSTRACT

This study identifies tropospheric precursors to downward (DW) and non-downward (NDW) propagating sudden stratospheric warmings (SSWs) and examines whether there is any difference between such events, other than internal tropospheric variability, using a large compendium of SSWs obtained from a chemistry-climate model. It is found that SSWs in general are preceded by a sustained period of upward wave activity originating in the lower troposphere, which is stronger for DW-propagating events, giving rise to a weaker Polar Vortex. The differences in wave forcing between DW and NDW events are associated with anomalous regional wave patterns in the troposphere; precursors that may aid in the prediction of DW and NDW events at the SSW onset. The DW influence of split and displacement events are also examined, finding that anomalous upward wave-1 fluxes are present in both cases, and that despite splits having a near instantaneous barotropic response in the stratosphere and troposphere, displacements have a stronger long-term influence. However, the identified precursors to DW and NDW SSWs do not become statistically significant until more modelled events than have been observed are composited. We finally compare these results to randomly-selected events independent of the SSW influence. This allows us to rule out that the tropospheric signal following some SSWs is attributable to just internal tropospheric variability, but rather confirms a DW influence from the stratosphere. Overall, these results suggest that the predictability of DW events could instead be enhanced by examining the strength of the regional anomalies which occur prior to the SSW.

1. Introduction

Approximately once every other year, the winter-hemisphere westerly stratospheric Polar Vortex weakens, reverses in direction and warms dramatically over the course of just a few days in a sudden stratospheric warming (hereafter SSW; see Butler et al. 2015, and references therein). Generally it is thought that such a SSW is caused by an anomalously strong upward flux of planetary waves from the troposphere (e.g., Matsuno 1971; Polvani and Waugh 2004; Sjoberg and Birner 2012), although it is not known if the reason for this upward flux is due to changes in the tropospheric wave forcing itself, or due to stratospheric circulation changes which can modulate the reservoir of wave activity below (e.g., Birner and Albers 2017; Garfinkel and Schwartz 2017). Due to the hemispherical differences in topography, all but one of the observed SSWs have occurred in the Northern hemisphere (NH) (e.g., Charlton and Polvani 2007).

It is acknowledged that SSWs can have an appreciable influence on the tropospheric circulation below for up to 2 months following the onset of the event (e.g., Baldwin and Dunkerton 2001; Polvani and Kushner 2002; Nakagawa and Yamazaki 2006; Mitchell et al. 2013; Hitchcock and Simpson 2014; Kidston et al. 2015). In particular, SSWs on average precede a persistent equatorward shift of the North Atlantic eddy-driven jet (i.e., a negative phase of the North Atlantic Oscillation [NAO]). The eddy-driven jet is colocated with the extratropical storm tracks, and hence plays a crucial role in determining the weather over North America and Europe (e.g., Kidston et al. 2015). Additionally, it has been shown that SSWs result in an increase in cold-air outbreaks in the midlatitude NH (Thompson et al. 2002; Tomassini et al. 2012) as well as high-latitude blocking events (Martius et al. 2009). Thus, it has been suggested that the skill of tropospheric seasonal forecasts can be improved by enhancing our understanding of SSWs and their downward influence on the tropospheric circulation (Marshall and Scaife 2010; Scaife et al. 2012; Smith et al. 2012; Sigmond et al. 2013; Tripathi et al. 2014).

Whilst there is a clear aggregate impact of SSWs on the troposphere, there is considerable variation between individual events (Baldwin and Dunkerton 2001; Sigmond et al. 2013). Indeed, some events exhibit no visible impact and hence this has led to studies defining SSWs as either 'downward' (DW) or 'nondownward' (NDW) propagating (Jucker 2016; Kodera et al. 2016; Runde et al. 2016; Karpechko et al. 2017). However, there is debate about whether there is an actual DW communication of information from the stratosphere, or whether the observed influence is related to variability inherent to the troposphere. Thus, in this study we utilise a series of runs from the Goddard Earth System Community Climate Model (GEOSCCM) yielding a large sample of nearly 1000 SSWs, to setup and subsequently reject the null hypothesis that there is no difference between DW and NDW propagating events other than internal tropospheric variability. We achieve this by identifying zonal-mean and regional precursors to DW and NDW-propagating SSWs and compare them to randomly-selected events based purely on the behaviour of the troposphere. This large sample size helps us to overcome the sampling uncertainty faced in many previous studies which has led to varying conclusions, which we discuss below.

Previous studies have highlighted the role of the stratosphere in determining the extent of the DW influence. It has been suggested that the type and magnitude of the wave forcing (be it wave-1 or wave-2) entering the stratosphere (e.g., Nakagawa and Yamazaki 2006), the type of SSW (split or displacement) which occurs (e.g., Mitchell et al. 2013; Seviour et al. 2013; O'Callaghan et al. 2014; Seviour et al. 2016), the depth to which the intial warming descends in the stratosphere (Gerber et al. 2009; Hitchcock et al. 2013), and the persistence of the SSW in the lower stratosphere (Hitchcock and Simpson 2014; Maycock and Hitchcock 2015) can all play a role, either individually or collectively, in determining the tropospheric response. For instance, Nakagawa and Yamazaki (2006) found that observed SSW events which were followed by a significant long-lasting tropospheric anomaly were associated with an enhanced upward flux of wave 2. Mitchell et al. (2013) and Seviour et al. (2013) found that the observed tropospheric response was dependent on the SSW type; split SSWs were associated with such a response, whereas displacement SSWs were not. However more recently, using a large compendium of modelled SSWs, Maycock and Hitchcock (2015) disagreed with this, instead finding indistinguishable surface signals. In particular, they suggested that the tropospheric impact was dependent on whether the lower-stratospheric circulation anomalies persisted; a point which was also proposed by Hitchcock and Simpson (2014) and Karpechko et al. (2017) using reanalysis data and a full chemistry-climate model, as well as by Jucker (2016) using idealised GCM experiments. Lehtonen and Karpechko (2016) and Karpechko et al. (2017) both indicated the role of enhanced upward-propagating planetary waves prior to the onset of the SSW as well as its continuation for a up to a week after the onset.

On the other hand, both observational and modelling studies have suggested that the troposphere plays a key role in determining the extent of the DW influence of the SSW. In particular, tropospheric precursors and the state of the tropospheric circulation can determine the initial forcing of the SSW (e.g., Martius et al. 2009; Garfinkel et al. 2010; Cohen and Jones 2011; Dai and Tan 2016; Hitchcock and Haynes 2016; Bao et al. 2017) as well as the ensuing tropospheric response (Black and McDaniel 2004; Hitchcock and Simpson 2014). In terms of observations, Black and McDaniel (2004), for instance, observed that the determination of the DW propagation of a SSW depended on the pre-existing tropospheric state; in the case of nondownward-(NDW)-propagating events, the troposphere was already in a positive NAM-like state which acted to mask the DW stratospheric influence. In the case of DW-propagating events, the troposphere was already in a negative NAM-like state, although slightly out of phase, latitudinally, with the canonical NAM. Further, Garfinkel et al. (2010) found that surface variability over the North Pacific and Eastern Europe could either deepen or flatten the troughs/ridges associated with tropospheric stationary planetary waves. Such precursors over these two regions then lead to changes in the upward wave flux and possibly the onset of a weaker Polar Vortex, followed by its DW propagation. Depending on the magnitude and spatial location of this anomalous forcing, either a split or displacement SSW may occur (e.g., Cohen and Jones 2011).

Modelling studies by Gerber et al. (2009) and Hitchcock and Simpson (2014) have shown that variability inherent to the troposphere may play a key role in determining the extent of the DW propagation. Using an idealised atmospheric general circulation model, Gerber et al. (2009) added random perturbations to the synoptic-scale vorticity field in the midlatitude troposphere in a 100-member ensemble forecast around a given event. They found that the same SSW event can either appear to influence the troposphere or not, just by allowing natural variability to spread the troposphere. Further, Hitchcock and Simpson (2014) utilised a chemistry-climate model and initialised the troposphere and stratosphere differently, with the stratosphere being nudged towards a reference zonal-mean SSW event and the troposphere being allowed to evolve freely. Even though the stratospheric state was essentially the same throughout the model integrations, in some integrations the SSW event reached down to the surface, whereas in others it did not. Sigmond et al. (2013) showed that whilst the mean NAM forecast shifts to be more negative, the spread does not decrease. This latter study by Sigmond et al. (2013) in combination with those by Gerber et al. (2009) and Hitchcock and Simpson (2014), indicate that tropospheric variability may be somewhat decoupled from the stratosphere, and that despite the SSW having a tendency to push the tropospheric NAM towards a negative state, the tropospheric response may depend on whether tropospheric variability acts to amplify or reduce the shift.

The paper is structured as follows: in section 2 we present a description of the GEOSCCM model integrations used in this study, and of the methods used to identify SSWs (Charlton and Polvani 2007) and split and displacement vortex events (Seviour et al. 2013), and also determine whether these events are DW or NDW propagating (Jucker 2016; Runde et al. 2016; Karpechko et al. 2017); in section 3 we present the results; and finally, in section 4 we present a summary and dicussion.

2. Methodology

a. Model Output

We utilise a series of model integrations which were performed using the Goddard Earth Observing System Chemistry-Climate Model, Version 2 (GEOSCCM; see Rienecker et al. 2008). The GEOSCCM couples the GEOS-5 (Molod et al. 2012) atmospheric general circulation model (GCM) with StratChem, a comprehensive stratospheric chemistry module (Pawson et al. 2008). In total, 40 historical-run integrations are here analysed, 25 of which are of length 30 years (January 1980 to December 2009) and 15 are of length 55 years (January 1960 to December 2014), which yields a total of 1575 years of data to analyse. These are described in more detail in Garfinkel et al. (2015), Aquila et al. (2016) and Garfinkel et al. (2017). The integrations were performed for different purposes and therefore this 'super ensemble' encompasses a range of forcings and physical parameterisations. These include changing sea surface temperatures, sea-ice and greenhouse gas concentrations, as well as ozone-depleting substances, solar variability, and volcanic eruptions. We note that there is a slight influence of SSTs on the DW and NDW propagation of SSWs, but it is comparatively weak and this is discussed in a future publication. We also note that the two different time periods (i.e., pre- and post-satellite era) over which the integrations are run do not have an influence on the results. The model was run using 72 vertical layers with a lid at 0.01 hPa, although we base our analysis on 15 levels ranging from 850 hPa up to 1 hPa. Additionally, the horizontal resolution is 2° latitude by 2.5° longitude.

b. SSW Definitions

To define SSW events in the GEOSCCM model integrations described above, we first utilise a simplifed version of the World Meteorological Organisation (WMO) criteria proposed by Charlton and Polvani (2007) where SSWs are defined by a reversal of $\overline{u}$ at 60°N and 10 hPa to easterly winds dfrom November 1^{nd} to March 31^{st}. This criterion is supplemented by the requirement that winds return to a westerly state for a period of 10 consecutive days prior to April 30^{th}, which helps avoid counting any final warmings, and a separation of at least 20 days between two consecutive events, to avoid counting the same SSW event twice (see also the corrigendum of Charlton and Polvani 2007). Note that for robustness, we have also performed the analysis using the Northern Annular Mode (NAM) index (as in Thompson et al. 2002), the NAM tendency index (as in Martineau and Son 2015) and the $\overline{u}$ tendency (as in Martineau and Son 2013; Birner and Albers 2017), finding qualitatively similar results. Using the SSW definition above, a total of 962 SSWs (see table 1) are found giving a ratio of 0.61 per year; a ratio not too dissimilar to that found in observations (also see table 1 in Butler et al. 2015).

We also identify the two characteristic types of extreme vortex variability - split and displacement SSWs - using the 2-D moment analysis method described by Seviour et al. (2013). In particular, the geopotential height Z at 10 hPa, rather than the potential vorticity as in Mitchell et al. (2013), is used in this method. Seviour et al. (2013) detail this method, but there are three parameters which are to be modified appropriately for this study. The first is the edge of the Polar Vortex, which we here define as the December-March (DJFM) climatological mean Z at 60°N and 10 hPa (as in Maycock and Hitchcock 2015), where the climatology is defined as the average over all DJFM winters in all 40 ensemble members. The second and third are the thresholds for the split and displacement SSWs, which depend on the values of the centroid latitude and aspect ratio. We here choose the thresholds as the most equatorward 5% of centroid latitudes and largest 5% of aspect ratios in all ensemble members, yielding thresholds of 64.3°N and 2.074 respectively (compare these values to the respective 5.7%/66°N and 5.2%/2.4 used in Seviour et al. 2013). We note that the results are not sensitive to slight changes in the thresholds used here. We also note that a handful of events satisfy both criteria, in which case they are marked as unclassifiable, to try and best ensure independent events. Using this method, we find a total of 903 events with 400 splits, 500 displacements, and 3 unclassified (see table 1). Note that these events are not the same as the 962 SSW events identified using the CP07 method, as we do not here classify the CP07-identified SSWs as splits or displacements.

c. DW- and NDW-propagating Event Definitions

To define whether a given event is DW or NDW propagating we utilise the NAM index. In this study we compute a simplified NAM index based on the polar-cap average geopotential height, Z. Standardised Z anomalies are calculated at each level as the deviation from the 60-day low-pass filtered daily climatology, which are subsequently smoothed using a 3-day running mean, following Martineau and Son (2015), although we note that quantitatively similar results can be found using different filtering windows. The anomalies are then area-averaged (i.e., multiplied by $\cos\varphi$) over 60-87°N, divided by the standard deviation at each level and multiplied by -1 so that conventionally, a negative NAM index identifies with a positive Z anomaly and vice versa.

Four definitions have been proposed recently to characterise the DW propagation of SSWs using the NAM index; one by Runde et al. (2016), two by Jucker (2016), and one by Karpechko et al. (2017). We quickly summarise each one here and refer the reader to table 1 for the numbers of DW and NDW-propagating events associated with each definition. First, Karpechko et al. (2017) introduced three criteria that must be satisfied, these being: 1) the averaged NAM index at 1000 hPa over the period ranging from 8 days until 52 days after the onset date must be negative; 2) the fraction of days in this 45-day period on which the NAM index at 1000 hPa is negative must be greater than 0.5; and 3) the fraction of days in this 45-day period on which the NAM index at 150 hPa is negative must be greater than 0.7. Note that for the first two criteria we use the NAM at 850 hPa to avoid complications with topography and for the third we use 100 hPa to ensure that the anomalies persist in the lower stratosphere, although we note that the results are not sensitive to the choice of level. These criteria are chosen to ensure that there is a long-lasting tropospheric signal of the negative NAM anomalies associated with the upper-tropospheric/lower-stratospheric negative anomalies.

Runde et al. (2016) proposed a more restrictive definition. In particular, the NAM index has to be more strongly negative than -1.5 standard deviations at every level below 10 hPa down to 850 hPa for at least one day in the succeeding 70 days (although we chose this window) after the onset date. Additionally, the date of the first exceedance of the threshold at each level must be after (or occur simultaneously to) the first exceedance at the level above. If this is not satisfied then the end date of the exceedance at a given level must occur after (or again simultaneously to) the end date at the level above. Further, the start lag of the threshold exceedance at a given level must be within 30 days of the end date of threshold exceedance at the level above, to try and ensure that the anomalies at each level are connected. Overall this ensures that there is a clear DW propagation from the middle stratosphere to the lower troposphere.

The two proposed definitions by Jucker (2016) will be referred to as the absolute-criterion and relative-criterion definitions herein. The absolute-criterion definition simply demands that the NAM index averaged over lags +10 to +40 be smaller than -0.6. We note, as they do, that our results are insensitive to changes in this window, as well as changes in the threshold value. On the other hand, the relative-criterion definition demands that the relative change of the NAM index at 500 hPa between positive lags (averaged over lags +1 to +80) and negative (averaged over lags -80 to -1) must be smaller than -0.1. We note again, that the results are not sensitive to the thresholds in this definition, aside from the fact that the averaging periods used influence the width of the positive and negative anomalies either side of the onset date in the composite plots (see figure 8).

One thing to be mindful of when identifying a given SSW as DW-propagating is to determine if the tropospheric NAM anomalies are actually attributable to those in the stratosphere. More specifically, the negative tropospheric NAM at positive lags could be due to either the stratospheric anomaly propagating DW, or, due to the persistence of a negative tropospheric NAM prior to the onset. Indeed, it could also be a combination of the two, or even the negative tropospheric NAM at positive lags spontaneously developing, unrelated to the stratosphere. Of course, to distinguish between all of these is very difficult, but from our sensitivity tests, the definitions by Karpechko et al. (2017) and Runde et al. (2016) go some way towards ensuring this, with particular emphasis on the latter which demands an apparent systematic DW propagation from the middle stratosphere to near the surface. Although we discuss the sensitivity of our results to the definitions in section 3b, we note here that the Karpechko and Runde definitions yield quantitatively similar results, and because the former gives a larger compendium of DW SSWs (see table 1), we choose to mostly utilise the definition by Karpechko et al. (2017) herein, unless explicitly stated otherwise.

3. Results

We start by examining the evolution of the tropospheric and stratospheric circulation and wave propagation during SSW events and identifying precursors to both DW and NDW propagating events. We then determine the robustness of the identified precursors using a variety of different DW definitions as well as comparing our results to randomly-selected tropospheric NAM events. Finally, we identify the differences between split and displacement-type extreme vortex events as well as their DW propagation to the troposphere.

a. Identification of Precursors; Wind Reversal Criterion

We first examine the evolution of the NAM index composited at lag zero according to the onset date of the SSW (first day for which $\overline{u}$ at 60°N and 10 hPa reverses to easterly; Charlton and Polvani 2007). We also here only show results using the DW definition of Karpechko et al. (2017) but note that the robustness of these results to DW definition is discussed in section 3b. Figure 1 shows the NAM index composited over a) all SSW events in all of the ensemble members (a total of 962; see table 1); b) all DW-propagating SSW events (506; as determined by the criteria in Section 2); c) all NDW-propagating SSW events (456); and d) the composite difference between the DW- and NDW-propagating events (hereafter DW-NDW). In the all event composite (a), the NAM index is similar to the canonical 'dripping-paint' pattern first highlighted by Baldwin and Dunkerton (2001) showing that the model used in this study produces realistic SSWs. The negative anomalies initialise around lags -15 to -10 above $\sim$250 hPa, and at lag zero maximise in the upper stratosphere. The negative anomalies propagate DW to the lower stratosphere over the next few weeks and start to recover in the upper stratosphere after lag +20, although those in the lower stratosphere persist until lag +60. Negative anomalies are visible in the troposphere for all positive lags, but with much smaller amplitude than those in the stratosphere.

Upon subdividing the total into DW- and NDW-propagating events (b and c), it can be seen that the DW events have a much stronger influence on the troposphere after lag 0, by construction, with negative NAM anomalies reaching down to near the surface and persisting for over 60 days. At positive lags, the DW composite (b) has magnitudes of around twice that of the total (a) in the troposphere, which is due to the cancellation between the negative DW anomalies and the weakly-positive NDW anomalies in (c). Further, the magnitude of the negative anomalies in the upper stratosphere is larger for the DW events, and those in the lower stratosphere persist for considerably longer during DW events. Finally, there are larger negative tropospheric anomalies in the DW composite compared to the NDW composite prior to lag zero, indicating tropospheric preconditioning. Such anomalies have been found before in a large compendium of SSWs by Gerber et al. (2010), Hitchcock and Simpson (2014, their figure 5e), Hitchcock and Haynes (2016), Jucker (2016), and in a large ensemble of SSW events using the Canadian Middle-Atmosphere Model by Karpechko et al. (2017). Hence, it appears that DW SSW events appear to be stronger in overall magnitude in both the troposphere and stratosphere, persist for longer in the lower stratosphere and have evidence of tropospheric preconditioning, in comparison to those which are NDW propagating. The robustness of these precursors are discussed in section 3b.

To examine the differences in upward wave activity between DW and NDW events, in figure 2 we show the height-time evolution of the vertical component of the Eliassen-Palm (EP) flux

$$F^{(z)} = \rho_0 a \cos\varphi \left(\left[f - \frac{1}{a\cos\varphi} (\overline{u}\cos\varphi)_\varphi \right] \overline{v'\theta'}/\overline{\theta}_z - \overline{w'u'} \right) \tag{1}$$

(Andrews and McIntyre 1978; Andrews et al. 1987), where φ and z are the latitude and log-pressure height coordinates, u, v and w are the zonal, meridional and vertical components of the wind, θ is the potential temperature, f, a and ρ_0 are the Coriolis parameter, Earth's radius and basic state density, and overbars and primes represent the zonal-mean and deviations from the zonal-mean, respectively. $F^{(z)}$ is averaged over the latitude band of 45-75°N and filtered for planetary waves 1-2 and as in figure 1, presented as composites over (a) all SSWs, (b) DW SSWs, (c) NDW SSWs, and (d) the DW-NDW difference. Overall, there are positive anomalies preceding the onset date extending back to lags ∼40-45 in the troposphere before propagating up into the stratosphere and persisting until lag -5 in the lower to middle stratosphere. For

DW events, this preceding wave flux is enhanced compared to NDW events, being of nearly double the magnitude. After the onset date, there are generally negative stratospheric anomalies indicating reduced upward wave activity. In the troposphere, the anomalies are of opposite sign between DW and NDW events; for the DW events, there are positive anomalies which we note are dominated by wave-2, whereas for NDW events, there are negative anomalies. This results in DW-NDW differences which are positive from $\sim$ lag -28 to +50, and extend from 850 hPa into the middle stratosphere, although after $\sim$+20, the differences are confined below 200 hPa. We note that these differences become less significant if synoptic waves are included in the composite.

These $F^{(z)}$ anomalies allow us to define certain lag stages in the evolution of the DW and NDW SSWs (see dashed vertical lines). The first is the preconditioning stage (hereafter PC) from lags -25 to -1, which is chosen as it represents the approximate duration of the significant tropospheric precursor DW-NDW differences, although we note that that the tropospheric and stratospheric anomalies intensify at around lag -15. The second is the onset stage (ONS) from lags 0 to +5, which is associated with continued (reduced) anomalous upward wave propagation in the stratosphere (troposphere). Finally, we classify the recovery stage (REC) over lags +6 to +50 which represents the approximate timescale over which the tropospheric DW-NDW differences disappear. Note that results in this paper are not sensitive to slight changes in the definition of these lags.

It is natural to ask if the zonal-mean NAM and wave-forcing anomalies thus far are indeed zonal, or project instead onto a more regional pattern. Figure 3 shows the latitude-longitude distributions of the geopotential height Z anomalies at 850 hPa averaged over the PC stage (top row), ONS stage (middle row), and REC stage (bottom row). The November-February climatology for each variable is superimposed as green contours and we note that the climatologies in these

GEOSCCM integrations agrees well with observations (e.g., Garfinkel et al. 2010).

In the PC stage, the Z anomalies for the DW (a) and NDW (b) composites show similar spatial patterns, with a clear wave-1 like structure consisting of negative anomalies northward of 60°N over the North Pacific and positive anomalies over Scandinavia and Europe. These negative (positive) anomalies project onto the climatological stationary planetary wave-1 centres of action, albeit slightly offset to the northeast (northwest), respectively. In the DW composite, the magnitudes of the anomalies are noticeably larger than in the NDW composite; in particular the positive anomalies over Northern Europe which are doubled in the DW composite. This difference in magnitudes is highlighted in the DW-NDW composite (top right) with negative and positive differences over the Aleutian Low sector and the Siberian High sector respectively. We also note the regions of positive and negative anomalies further equatorward over the North Pacific and North Atlantic respectively. Over the North Atlantic, the anomalies are significantly more negative for the DW events.

During the ONS stage (middle row), positive anomalies appear over the Polar cap with an annulus of negative anomalies starting to develop at midlatitudes for the DW events. For the NDW events however, positive and negative anomalies develop over the Aleutian Low and Siberian High regions, respectively, projecting negatively onto the climatological centres and suggesting a reduced upward wave-1 flux. This yields differences which still show a wave-1 pattern over the North Pacific and Siberia, along with more widespread negative differences over the North Atlantic (compared to during the PC stage). The latter highlights the canonical DW influence of SSWs. The NAM at lags 0 to +5 is not utilised in the Karpechko et al. (2017) DW definition and hence these anomalies are not forced by the averaging associated with the definition. During the REC stage (bottom row), the strongest anomalies are associated with the DW events (indeed, with much smaller anomalies in the NDW composite), which exhibit a highly zonal pattern, with positive anomalies at high latitudes surrounded by an annulus of negative anomalies at midlatitudes, projecting onto the negative phase of the NAO. We note however, that these are present by construction.

In order to determine if the anomalous geopotential heights seen in figure 3 result in enhanced upward wave activity (as we ascertained) we calculate the vertical component of the 'Plumb flux'

$$F_p^{(z)} = \frac{p\cos\varphi}{p_s}\left(\frac{f}{N^2}\left[v'T' - \frac{1}{2\Omega a\sin 2\varphi}\frac{\partial}{\partial\lambda}(T'\Phi')\right]\right) \tag{2}$$

(Plumb 1985), where λ is the longitude, T the temperature, Φ the geopotential, N^2 the static stability, Ω the Earth's rotation rate, p the pressure, p_s the reference pressure level and v is here calculated using the geostrophic wind approximation ($v = (a\cos\varphi)^{-1}\partial\Phi/\partial\lambda$). Note that it has been written in this form so as to remove the presence of higher-order derivatives, to which the calculation can be sensitive. The primes represent deviations from the zonal-mean. This allows one to analyse the horizontal variations in the upward wave activity at a given level.

Figure 4 shows the same as figure 3 except for $F_p^{(z)}$ at 150 hPa. During the PC stage (top row), positive anomalies are present in the DW and NDW composites northward of 40°N. The main difference between the two is in magnitude; this is indicated in the DW-NDW difference where there are positive differences over Asia, the North Atlantic basin and the Eastern Pacific, and also negative differences over Eastern Europe. Although these anomalies enhance the climatological upward wave activity (green contours) under both DW and NDW events (indeed, leading to the SSW), it is particularly increased under DW events. We also note that the anomalies are dominated by wave-1 (not shown). This is in agreement with the 850-hPa Z anomalies in figure 3 wherein the anomalies enhanced the wave-1 centres of action. In the ONS stage (middle row), the structure is also similar to the EO stage, except that the magnitudes have decreased. Finally, in the REC stage, the upward wave activity is much reduced for both DW and NDW events, with generally negative anomalies everywhere for the NDW events. For the DW events, there are still weak positive anomalies over the North Atlantic and flanking the climatological peak over the Pacific and Siberia, indicating continued weak upward propagation.

In order to determine the vertical extent of the Z anomalies, we show longitude-height cross-sections of Z' (i.e., the deviation from zonal-mean) in figure 5, averaged over the same lag stages as in figure 3 and over the latitude band of 50-60°N. This latitude band is chosen as it best captures the negative and positive anomalies over the Aleutian Low and Siberian High regions shown in figure 3. In the climatology (thin black contours), there is a clear westward tilt with height of Z' agreeing with the well-known westward tilt with height of upward-propagating planetary waves (e.g., Andrews et al. 1987). The Z' has a wave-1 structure in the stratosphere with one ridge and one trough, but is associated with higher wavenumbers in the troposphere (multiple ridges and troughs). This agrees with the Charney-Drazin criterion (Charney and Drazin 1961) which states that only planetary waves can propagate into the stratosphere and smaller-scale waves are limited to propagation in the troposphere.

During the PC stage (top row), the anomalies for both DW and NDW events project positively onto the climatological Z' anomalies and exhibit the canonical westward tilt with height, indicating anomalous upward wave propagation from the troposphere to the lower-to-middle stratosphere. In particular, in the troposphere, there are negative anomalies spanning from 70°E eastward to $\sim$150°W, and positive anomalies from 150°W eastward to $\sim$60°E. These agree with the Z' anomalies at 850 hPa shown in figure 3. In the difference plot, it is clear that the anomalies associated with DW events are generally larger in magnitude indicating enhanced upward wave propagation.

After the onset date (middle row), the anomalies above 10 hPa change sign, thus projecting negatively onto the climatological centres. This could either be associated with reduced upward wave propagation deep into the stratosphere after a SSW event, in agreement with the Charney-Drazin criterion, or be directly related to the Z' anomalies associated with the weakened Polar Vortex. In the case of the latter, it likely represents the wave-1 pattern associated with (displacement) SSWs (see section 3c), which is therefore stronger for the DW events. Below 50 hPa, the anomalies and differences look generally similar to during the PC stage although slightly more connected, suggesting continued upward wave propagation into the lower stratosphere. During the REC stage (bottom row), the anomalies above 50 hPa deepen and intensify compared to during the ONS stage, which is particularly enhanced during the DW events. This is in agreement with a stronger SSW event (figure 1). Below 50 hPa, they lose their westward tilt with height, instead either exhibiting more of an eastward tilt, particularly over the North Pacific (g), or vanishing almost entirely (h). This indicates suppressed wave propagation into the stratosphere.

To further indicate the influence of the upward wave activity from the troposphere on the strength of the polar vortex, we plot a scatter graph of the vertical component of the Eliassen-Palm (EP) flux $F^{(z)}$ at 100 hPa and averaged over negative lags -15 to -1, against the NAM index at 10 hPa averaged over positive lags +1 to +10, in figure 6a. As in figure 2, $F^{(z)}$ is filtered for planetary waves 1 and 2 and averaged over 45-75°N. As aforementioned, we use lags -15 to -1 for $F^{(z)}$ as the EP flux intensifies during these lags in the stratosphere and troposphere (figure 2). We note that the window for $F^{(z)}$ used here is shorter than that used in Polvani and Waugh (2004) who found that a time-integrated upward flux over 40 days at 150 hPa gave the best correlation. Overall, as expected, an increase in upward wave activity leads to a decrease in the vortex strength, with a correlation coefficient of -0.60 which is highly significant ($p \ll 0.01$). Upon splitting into DW and NDW events, and calculating the lines of best fit for each, it can be seen that the respective correlation coefficients are also both very similar (-0.60 and -0.57). The composite mean for both event types (large squares) indicate that for DW events, there is a slightly larger upward flux of wave activity entering the stratosphere preceding the SSW, which results in a more negative NAM index at 10 hPa. Nevertheless, we note that there is still scatter about the lines of best fit, indicative of the high variability in the winter stratosphere. This could imply that a linear fit is not optimal, but we note that a nonlinear fit does not yield an increase in the R^2 value (which is here 0.36 for DW and 0.32 for NDW). Note that the correlation coefficients are robust only at levels close to 100 hPa, whereas closer to the surface, the correlations become smaller.

In figure 6b we also show a scatter plot of the lower-stratospheric $\overline{u}$ at 150 hPa averaged over lags +1 to +40 against the NAM index at 850 hPa averaged over the same period. Note that in this plot, the SSWs are classified as DW and NDW using the absolute-criterion definition of Jucker (2016), who defines such events using the NAM at 500 hPa. This limits the influence of the DW definition on the stratospheric and tropospheric NAM index as would be the case using the definition of Karpechko et al. (2017). A clear overall positive correlation is found (r=0.8) which is highly significant ($p \ll 0.01$). There is a clear separation between the DW and NDW events, as expected due to the DW events being defined as such, with more of a negative NAM in the upper troposphere-lower stratosphere and near to the surface compared to the NDW events. Nevertheless, some of the NDW events do have a negative near-surface signal, indicating that either there were lower-tropospheric negative NAM events occurring simultaneously to the given SSW, or this definition cannot identify all such events as DW-propagating. The correlation coefficients for the DW (NDW) events are both high at r=0.62 (r=0.61), although it is noticeably smaller than the overall correlation coefficient. Note that the correlation coefficients between $\overline{u}$ at pressure levels higher into the stratosphere against the NAM at 850 hPa, decrease with height. Hence, despite the SSW in the middle stratosphere being stronger for the DW events on average due to enhanced upward wave activity (figure 1), the tropospheric response is more dependent on the subsequent strength and persistence of the SSW in the lower stratosphere (Maycock and Hitchcock 2015), although the lower-stratospheric NAM response is in turn related to the strength of the NAM in the midde stratosphere (not shown).

It is worthwhile to examine how many SSWs are required to find precursory features such as those found in figures 1- 5. For instance, these precursor features to DW and NDW events are not found in reanalysis products such as the ERA-Interim reanalysis (see figure 1 in Karpechko et al. 2017), but they have been found in the zonal-mean sense in larger-samples obtained from GCMs (e.g., figure 3 in Karpechko et al. 2017). Hence in figure 7 we plot confidence intervals of the DW-NDW difference for the PC stage (-25 to -1) of (a) the NAM index at 300 hPa, (b) $F^{(z)}$ at 150 hPa averaged over 45-75°N, and (c) Z at 850 hPa area averaged over 50-80°N, 60-90°E, i.e., the positive differences slightly northwest of the climatological Siberian High. The confidence intervals are estimated using a Monte-Carlo repeat sampling procedure (100,000 repetitions), for different prescribed sample sizes. The confidence intervals for the 90% (red), 95% (green) and 99% (blue) levels all converge to the overall composite mean shown in the corresponding figures (see dotted black lines), as the sample size is increased from the minimum of 10 considered here, to the maximum of 455. From the definition of a confidence interval around the difference between the means of two samples, if the interval does not contain zero, then the means must be significantly different from zero, at the chosen level. Hence, we can ascertain from figure 7 that the point at which the upper bound crosses the zero difference line to become negative, is the approximate number of SSWs that are required to obtain the required level of statistical significance (see the respective coloured vertical lines).

In terms of the NAM index, it can be seen that at the 90%, 95% and 99% levels, the number of DW and NDW SSWs each required is ∼50, 70 and 110, respectively. For $F^{(z)}$, the numbers required are slightly less (∼45, 65, and 100), and for Z over the Siberian high sector, the numbers are much reduced (∼35, 45, and 75). In all three cases, even at the 90% level, the number of DW and NDW SSWs required separately to find such precursor anomalies, is more than that which is currently available in reanalysis datasets. We hence conclude that using a regional parameter such as the Z anomalies averaged over the Siberian High sector, may be a better indicator of whether an event will be DW or NDW propagating.

b. Robustness of Precursors

As there have been a variety of definitions used to diagnose DW propagation, we here test the robustness of the zonal-mean precursors found in figure 1 using each of the definitions introduced previously in section 2c. Figure 8 shows the NAM index at 500 hPa for the DW definition of Karpechko et al. (2017) (red line; also see figure 1), Runde et al. (2016) (blue line), and the absolute- and relative-criterion definitions of Jucker (2016) (green and black lines, respectively). We first note that at positive lags, all definitions show negative NAM for DW events by construction, although with differing magnitudes depending on the thresholds used in the individual definitions. At negative lags, the Karpechko, Runde and absolute-criterion definitions give quantitatively similar results to one another, with the DW composite showing negative NAM values prior to lag zero, and the NDW composite showing positive values from approximately lag -20 to 0 and negative values beforehand. This gives differences that are therefore negative and statistically significant extending back to approximately lag -25.

The relative-criterion definition gives drastically different results however for the DW and NDW composites prior to lag zero; positive anomalies for DW events and negative anomalies for NDW events, yielding positive differences prior to lag zero. The differences are antisymmetric (although the negative NAM at positive lags is of larger magnitude) around the central date and this is found to depend on the averaging window used to determine the DW propagation; in this example we used lags -40 to -10 and lags +10 to +40 as the averaging periods. This also agrees with Jucker (2016) who showed a similar composite centred on lag zero.

The differences in the NAM evolution among the four definitions can be related to the periods of time used in each definition. For instance, the Karpechko, Runde, and absolute-criterion definitions only use values of the NAM at positive lags, whereas the relative-criterion uses NAM values at both negative and positive lags. In regards to the former three, they can be used to identify precursor features at negative lags (and in fact, the Karpechko definition can be used up until lag +7) as required for this study, as they do not force the composites at such lags. In the case of the relative-criterion definition however, any precusors may be influenced by the definition. For this reason, we believe that the precursors are robust but we note that they are sensitive to the type of definition used.

Also shown on figure 8 is the composite NAM index consisting of random tropospheric events (cyan line). These random events are selected to test the null hypothesis aforementioned in the introduction; i.e., that there is a difference between DW and NDW events other than tropospheric variability. In order to calculate this random composite, we removed each SSW event and its surrounding 100 days (hence, 101 days total for each event) from the timeseries for each experiment, and then randomly selected a new event, which by construction, is unrelated to a SSW. We define each event as having a negative (Tneg) or positive (Tpos) tropospheric NAM after the 'onset date' by averaging the tropospheric NAM at 500 hPa over lags +10 to +50, yielding 411 Tneg and 551 Tpos events. Overall, the Tneg composite is negative at both positive and negative lags, whilst the opposite is evident in the Tpos composite. This yields differences that are significantly negative at all lags, and is remarkably similar to that found in the SSW differences, albeit with differences in magnitude at negative lags. However, we note that these events are randomly chosen and the onset date has no influence on the tropospheric NAM; indeed, the onset date could be randomly chosen to either occur at the start, in the middle, or at the end of the lifecycle of the negative tropospheric NAM event, which when averaged over all 962 events, would conceivably give a composite similar to that shown in figure 8. In fact, upon reselecting events hundreds of times, similar composites are found. Nevertheless, this viscerally highlights that the differences at positive lags in the troposphere are entirely there by construction.

Although in the zonal-mean, the random composites show negative differences prior to the 'onset date' (extending back to lag -60), they may not be associated with enhanced upward wave forcing as was the case with the SSW composites (figure 3a-c). Figure 9 shows the GPH anomalies at 850 hPa for the DW and NDW SSW events (left column; reproduced from figure 3a,b), the Tneg and Tpos events (middle column), and the differences DW-Tneg (right column, top) and NDW-Tpos (right column, bottom). The Tneg events show overall much weaker anomalies than the DW SSW events with negative anomalies at midlatitudes associated with a localised trough over the North Pacific basin and a smaller-valued trough over the North Atlantic basin, and positive anomalies further poleward. This yields DW-Tneg differences with a high slightly northwest of the climatological Siberian High and a low slightly to the northeast of the climatological Aleutian Low, similar to figure 3c due to the dominance of the SSW composites. In terms of the Tpos events, there is also a more annular structure, but of opposite sign to the Tneg events, yielding annular and opposite-signed differences to DW-Tneg. Hence, the precursor anomalies associated with DW and NDW SSWs which are related to stationary planetary wave-1 forcing, are not similar to those associated with randomly-selected Tneg and Tpos events. This allows us to reject the null hypothesis aforementioned, and conclude that the regional patterns represent real differences between DW and NDW- propagating events, distinct from tropospheric variability.

c. Precursors to Splits and Displacements

Recent studies have highlighted the importance of the type of vortex event - be them either split or displacement events - on the surface observed after the onset of the event. In particular, Mitchell et al. (2013) and Seviour et al. (2013) found using the ERA-40 and ERA-Interim reanalyses that split events have a larger and more observable surface impact compared to displacements. In order to determine if there is any link between the tropospheric precursors which we found in sections 3a and 3b and the type of event, we here classify the split and displacement events as either DW or NDW propagating using the DW definition of Karpechko et al. (2017).

Figure 10 shows the height-time evolution of the NAM index divided into displacements (left column) and splits (middle column) and subdivided further into the total (top row), DW-propagating (middle row) and NDW-propagating (bottom row). Also shown are the differences (right column) for displacements-splits (top), DW-NDW displacements (middle) and DW-NDW splits (bottom). In the total composites, clear significant differences between displacements and splits can be seen in both the stratosphere and in the troposphere. In the stratosphere, the displacements are stronger than the splits, up until lag +50. In particular, in the middle-to-upper stratosphere the displacements are nearly twice as strong. In the troposphere, whilst the displacement events have a stronger long-term influence up until lag +45, the splits have a more barotropic nature at the onset with an instantaneous response near the surface, which dissipates after $\sim$lag +5. The barotropic nature at the onset is in agreement with the more likely role of the barotropic mode for split SSWs (Esler and Scott 2005). Prior to the onset date, the splits show clear tropospheric negative anomalies extending back to lag -45 which are stronger than for the displacements. Further, these split anomalies are nearly of equal strength to those which occur at positive lags, indicating that such events may actually have less of an influence on the troposphere, at least in this zonal-mean sense.

Upon subdividing into DW (middle row) and NDW (bottom row) events, the splits and displacements broadly show similar results to those found using the wind reversal criterion (figure 1) with slightly stronger negative NAM anomalies in the middle to upper stratosphere as well as longer-persisting anomalies in the lower stratosphere for DW events. This yields therefore, similar DW-NDW composite differences at positive lags to figure 1. However, at negative lags, the splits have much stronger negative tropospheric and lower-stratospheric precursors than the displacements, extending back to lag -55 and becoming stronger around lag -25 for the DW events, but weaker anomalies extending back to lag -30 for the NDW splits. The DW displacements on the other hand show very similar anomalies to the total (a), and the NDW displacements show evidence of positive tropospheric anomalies up to two weeks before the onset (and weakly negative anomalies before that). Overall, this gives similar-valued DW-NDW differences at negative lags, except that the splits have negative differences which extend further back to lag -30 and also extend into the stratosphere.

As before, we now examine the regional differences in order to understand these tropospheric precursors. Figure 11 shows the same as figure 3 except for Z at 850 hPa for the displacement events. At negative lags, there are negative anomalies over the Northwestern Pacific and positive anomalies over Northern Europe and Siberia. These two anomalous centres project onto the climatological wave-1 centres of action (green contours), and in particular, the positive anomaly over Northern Euope/Siberia is stronger for the DW events, indicating similarly to figure 3, an increase in upward wave-1. Also over the subtropical North Pacific, there is a band of positive anomalies projecting onto the eastern flank of the climatological wave-1 Aleutian Low. These anomalies are stronger under NDW events and hence yield negative differences over the Aleutian Low sector. This subtropical band of positive anomalies in conjunction with the negative anomalies further poleward, yield a dipole over the Pacific basin leading to possible meridional shifts in the East Pacific Jet (e.g., Nishii et al. 2010; Dai and Tan 2016; Bao et al. 2017). During the ONS and REC stages, the anomalies are very similar to as in figure 3, with a more zonal structure as the lag progresses and displaying evidence of reduced upward wave propagation under NDW events compared to DW events in the REC stage.

Figure 12 shows the same as figure 11 except for the split events. In contrast to the displacement events, the anomalies at this level show more of a wave-2 structure, with an intensification of the highs and lows of the climatological wave-2 (green contours). In particular, there are negative anomalies over the North Pacific, over the North Atlantic and Western Europe, along with positive anomalies over Siberia and Eastern Europe. In general, these anomalies are stronger for the DW events, as indicated by the difference composite. The differences also show evidence of an intensification of the climatological wave-1. During the ONS stage, the anomalies become more pronounced with a noticeable increase in magnitude. Both the DW and NDW composites show a wave-2 pattern, although this is even more clear for the NDW events. The DW events also show a projection onto the climatological wave-1 centres with negative anomalies over the Aleutian Low and positive anomalies over Siberia. During the REC stage, the DW composite at high latitudes looks similar to during the ONS stage, in agreement with the near-barotropic structure shown in figure 10. In the REC stage, although the DW anomalies are more annular (by construction), there is enough of a break from asymmetry to project positively onto the climatological wave-2, indicating an enhanced upward flux. Under NDW events, the anomalies are negligible in comparison.

We now plot the height-time evolution of $F^{(z)}$ for displacement events (figure 13) and split events (figure 14) in order to determine the vertical extent of the wave-1 (top row) and wave-2 (bottom row) anomalies from the troposphere into the stratosphere. Prior to the onset, there is enhanced upward wave-1 under DW events, which propagate up from 850 hPa into the lower stratosphere near 50 hPa. After the onset, the wave activity is generally suppressed as shown by negative anomalies in both the DW and NDW events, although positive (upward) anomalies do persist in the upper troposphere to lower stratosphere for a short while ($\sim$5 days) after the onset. The negative anomalies for the NDW events are of significantly larger magnitude. Additionally, after the onset (around lag 10 or so) there is significantly enhanced upward wave-2 in the troposphere (up to 400 hPa) for DW events, in agreement with figure 2. Note that the other wavenumbers contribute negligibly to the F_z flux and hence we do not include them here, for brevity.

For split events (figure 14), we can see that they are generally preceded by large upward wave-2 anomalies which propagate up from 850 hPa and peak in the middle to upper troposphere, with only a small amount penetrating into the stratosphere at the onset date. This is the case for both DW and NDW events (d and e), although there are actually slightly less upward wave-2 at the onset for the DW events (panel f; opposite to Nakagawa and Yamazaki 2006). However, those which propagate DW to the troposphere are preceded by enhanced anomalous upward wave-1 into the stratosphere compared to NDW events (see a and b). In the differences (c) it can be seen that this enhanced upward wave-1 starts around lag -20 and persists through the onset date until around lag +10. Even though split events are generally associated with wave-2 anomalies in the upward flux (as shown in d and e), this result indicates that in order for a split event to propagate DW, there must also be anomalous wave-1 fluxes. Similar to the displacements, there are enhanced upward tropospheric wave-2 anomalies for the DW events after the onset date.

4. Summary and Discussion

Using a series of 40 integrations of the GEOSCCM model, we have examined differences between so-called downward (DW) and nondownward (NDW) propagating SSWs. We have (1) established the existence of tropospheric precursor circulation anomalies to DW and NDW events, which manifest as nonzonal wave patterns which project onto the climatological stationary-planetary wave centres and also onto the zonal-mean NAM, and (2) demonstrated that these precursors are intimately connected with upward and downward coupling between the stratosphere and the troposphere, not simply related to variability inherent to the troposphere. To do this we identified a large compendium of SSWs across all of the 40 runs by using the definition of Charlton and Polvani (2007). This yielded a realistic ratio of approximately 0.61 SSWs per year ($\sim$950 in $\sim$1600 years) which should be compared with reanalysis datasets such as the ERA-Interim, which has a ratio of 0.69 (e.g., Butler et al. 2015). These SSW events were then classified as DW and NDW-propagating using a variety of recently-developed DW definitions (Jucker 2016; Runde et al. 2016; Karpechko et al. 2017).

For the SSWs in general, there is enhanced upward wave activity into the stratosphere from the troposphere, which appears to originate in the middle-to-lower troposphere near 850 hPa (figures 2- 6 and 11- 14), the lowest level that is considered here. This occurs as a projection of the anomalies onto the climatological centres of action, associated with a deepening of the Aleutian Low and a strengthening of the Siberian High and yielding an enhanced upward wave-1 flux. This upward flux is evident around lags -40 to -30, but intensifies around lag -15, propagating upward from the troposphere and into the stratosphere and likely contributing to the onset of the SSW (e.g., Matsuno 1971; Polvani and Waugh 2004). The enhancement of upward wave-1 activity prior to the onset, followed by the proceeding reduction at later times is in agreement with the observational composites of Limpasuvan et al. (2004) using reanalysis data.

A recent study by Birner and Albers (2017) found that SSWs are generally not preceded by lower-tropospheric wave-activity anomalies, but instead caused by the stratosphere 'tapping-in' to the reservoir of tropospheric wave activity below. In particular, they found that only 25% of the SSWs in the ERA-Interim reanalysis were preceded by enhanced lower-tropospheric wave activity and hence for the majority of SSWs, the anomalous upward wave fluxes generally occur in the stratosphere, and not in the troposphere. Here, we note that there is also a statistically-significant enhancement of wave activity even in the lower troposphere if at least 35 events of each type are considered (figure 7). However, given the large amount of internal variability (figure 6), we acknowledge that enhanced lower-tropospheric wave activity alone is not sufficient to predict whether a SSW will be DW or NDW-propagating.

In the case of DW-propagating SSWs, we find evidence of both significantly enhanced zonal-mean and regional tropospheric precursors, compared to the NDW SSWs. In terms of the zonal-mean, negative NAM anomalies are found to exist in the troposphere prior to the onset date for DW events, with negative DW-NDW differences extending as far back as lag -40 (see figure 1). Zonal-mean precursors were also found previously by a suite of studies (e.g., Gerber et al. 2009; Hitchcock and Haynes 2016; Jucker 2016; Karpechko et al. 2017), all of which utilised model output to identify large numbers of SSWs. In a regional sense, these negative NAM anomalies manifest as changes in the geopotential height (figure 3) and hence upward wave activity (figures 4 and 5) at lower levels and throughout the troposphere and lower stratosphere, which strengthen the wave anomalies already associated with the onset of the SSW. The upward wave activity is particularly strong over Northern Europe and Siberia, with a strengthening of the climatological Siberian High under DW events.

The enhanced upward wave activity associated with the DW-propagating events gives rise to a significantly weaker Polar Vortex in the middle stratosphere (figures 1, 5 and 6). However, as found by Runde et al. (2016) and despite the strength of the initial anomaly in the middle stratosphere (in their study they used 30 hPa) being stronger, the DW influence of the SSW is more dependent on the SSW anomalies in the lower stratosphere (figure 6b; also in agreement with Christiansen 2005; Gerber et al. 2009; Hitchcock and Simpson 2014; Maycock and Hitchcock 2015; Karpechko et al. 2017). However, we note that the initial anomaly in the middle stratosphere may indeed influence the persistence of the SSW anomaly in the lower stratosphere.

Using a Monte Carlo repeat-sampling procedure we determined the numbers of DW and NDW SSWs that are separately required to obtain the zonal-mean and regional precursors that have been found in this study. Of the three presented variables (see figure 7), the regional Z anomalies averaged over the Siberian High sector yielded the smallest number of required SSWs in order to find statistically significant differences between DW and NDW events. However, in all three cases, the number of SSWs required is more than that which is currently observed in reanalysis datasets to obtain significance even at the 90% level. This may explain why such precursor patterns have not been previously observed in studies using smaller sample sizes.

To rule out that the DW events were simply related to persistent negative tropospheric NAM events which happened to occur around the time of a SSW and hence manifest as tropospheric precursors, we tested the robustness of our results using a variety of different DW definitions

(Jucker 2016; Runde et al. 2016; Karpechko et al. 2017). Of these definitions, that by Runde et al. (2016) perhaps best ensures an apparent DW propagation from the stratosphere to the lower troposphere, ruling out any events for which the tropospheric NAM was already negative, by looking at the timing and magnitude of the negative NAM (specifically, with the NAM less than a chosen threshold) at each level (section 2c). Nevertheless, the results using the Karpechko et al. (2017) definition, the Runde et al. (2016) definition, and the absolute-criterion definition by Jucker (2016) were all quantitatively similar (figure 8), also giving gravitas to the existence of the identified precursors. However, our results were sensitive to the type of DW definition, with the relative-criterion definition of Jucker (2016) giving opposite-signed results at negative lags. We note that this is related to the lags which are used in each definition; the first three utilise only the NAM at positive lags, whereas the latter uses both positive and negative lags, somewhat precluding the identification of any precursors. Nevertheless, we conclude that our results do show evidence of a robust DW propagation from the middle stratosphere to the troposphere, and hence can negate the idea that the DW SSW events simply coincided with periods of extended negative tropospheric NAM.

In order to further negate the null hypothesis that differences between DW and NDW events reflect internal tropospheric variability, we compared the SSW composites to composites consisting of randomly-selected tropospheric events which are independent of the influence of SSWs. These events were selected by removing each SSW event and its surrounding days from the timeseries and then choosing a random day in the remaining winter days to be the central date of the tropospheric event (note that the central date is therefore arbitrary; see section 2c) These tropospheric NAM events were subsequently divided into positive (Tpos) and negative (Tneg) events. In a zonal-mean, the composites for the DW and NDW SSWs and for the Tneg and Tpos random events were remarkably similar (figure 8). However, the regional precursors (figure 9), which were found to be associated with upward wave forcing for the SSW events, were very different for the random composites, instead having a weak, annular structure and indicating an alternative meaning to the precursors. The replicability of the tropospheric zonal-mean NAM at both positive and negative lags using random events based solely on the behaviour of the troposphere, suggests exhibiting caution to just using the NAM to examine the DW influence of a SSW event, as it can conceal much of the regional information that is important for understanding the precursors. Nevertheless, because of the differences in the regional tropospheric precursors between SSW events and randomly-selected events, we therefore conclude that there is a difference between DW and NDW events aside from just internal tropospheric variability.

We also examined the evolution of the troposphere and stratosphere associated with split and displacement SSW events. We found that displacements tend to have a longer-term tropospheric influence whereas splits have a more barotropic influence at the onset date (figure 10). Such a barotropic influence is in agreement with the barotropic mode leading to a split SSW (Esler and Scott 2005; Matthewman et al. 2009; Seviour et al. 2016). However, these results disagree with studies by Mitchell et al. (2013), Seviour et al. (2013), O'Callaghan et al. (2014) and Lehtonen and Karpechko (2016) who found that splits have a larger tropospheric influence than displacements in reanalysis data lasting up until lag +60. The disagreement may be related to the differences in sample sizes which is an order of magnitude larger in our study. Indeed, we created composites for each individual experiment (not shown), and in a handful of the 40 ensemble members, composites are qualitatively similar to Mitchell et al. (2013). However, we note that our results are more in agreement with Seviour et al. (2016), who used 13 stratosphere-resolving models from the fifth Coupled Model Intercomparison Project (CMIP5) ensemble and found that despite splits exhibiting a slightly stronger signal over the North Atlantic for up to one month after the SSW, the largest and most significant differences were associated with displacements over Siberia. We note that our results therefore, are also slightly in disagreement with Maycock and Hitchcock (2015) and Karpechko et al. (2017), who in their large ensemble of SSWs obtained from a chemistry-climate model, instead found indistinguishable differences between the two types of events.

Despite the splits and displacements being associated with enhanced upward wave-2 and wave-1 forcing respectively (e.g., Andrews et al. 1987; Nakagawa and Yamazaki 2006; Liu et al. 2014; Lehtonen and Karpechko 2016), we also found that those splits and displacements which propagate DW to the troposphere are associated with even further enhanced wave-1 fluxes as compared to NDW-propagating events. As was the case with the general SSWs, evidence of this anomalous wave forcing was seen in the middle-to-lower troposphere.

As shown in our paper, the strength of the underlying tropospheric wave forcing, related to non-zonal wave precursors, and consequently the strength of the polar vortex, influences whether a SSW event will be DW or NDW-propagating. These precursors may allow predictability of whether a SSW event will be DW or NDW propagating to be possible up to a few weeks before the onset, although given the large amount of internal variability associated with the tropospheric wave flux (figure 6a), we note that it is difficult to know for what given wave forcing, a DW SSW may occur. Currently, we are investigating whether there is indeed any potential for predictability of DW or of NDW events in advance of a particular season, and hence aid in seasonal forecasting, and we plan to discuss these results in a future publication. We also note that our results are only based on the output from one model (GEOSCCM) and hence, the precursors which we here find must be verified using observations as well as other models.

Acknowledgments. We wish to thank useful conversations with Hella Garny, Alexey Karpechko and Amanda Maycock. We also acknowledge the support of a European Research Council starting grant under the European Union Horizon 2020 research and innovation programme (grant agreement number 677756).

References

Andrews, D. G., J. R. Holton, and C. B. Leovy, 1987: *Middle Atmosphere Dynamics*. Academic Press, 489 pp.

Andrews, D. G., and M. E. McIntyre, 1978: Generalized Eliassen-Palm and Charney-Drazin theorems for waves on axisymmetric mean flows in compressible atmospheres. *J. Atmos. Sci.*, **35**, 175–185.

Aquila, V., W. H. Swartz, D. W. Waugh, P. R. Colarco, S. Pawson, L. M. Polvani, R. S. Stolarski, and D. W. Waugh, 2016: Isolating the roles of different forcing agents in global stratospheric temperature changes using model integrations with incrementally added single forcings. *J. Geophys. Res. Atmos.*, **121**, 8067–8082.

Baldwin, M. P., and T. J. Dunkerton, 2001: Stratospheric harbingers of anomalous weather regimes. *Science*, **294**, 581–584.

Bao, M., D. L. Hartmann, and P. Ceppi, 2017: Classifying the tropospheric precursor patterns of sudden stratospheric warmings. *Geophys. Res. Lett.*, **44**.

Birner, T., and J. R. Albers, 2017: Sudden stratospheric warmings and anomalous upward wave activity flux. *Sci. Onl. Lett. Atmos.*, **13A**, 8–12.

Black, R. X., and B. A. McDaniel, 2004: Diagnostic case studies of the northern annular mode. *J. Clim.*, **17**, 3990–4004.

Butler, A. H., D. J. Seidel, S. C. Hardiman, N. Butchart, T. Birner, and A. Match, 2015: Defining sudden stratospheric warmings. *Bull. Amer. Meteor. Soc.*, **96**, 1913–1928.

Charlton, A. J., and L. M. Polvani, 2007: A new look at stratospheric sudden warmings. Part I: Climatology and modeling benchmarks. *J. Clim.*, **20**, 449–469.

Charney, J. G., and P. G. Drazin, 1961: Propagation of planetary scale disturbances from the lower into the upper atmopshere. *J. Geophys. Res.*, **66 (1)**, 83–109.

Christiansen, B., 2005: Downward propagation and statistical forecast of the near-surface weather. *J. Geophys. Res.*, **110 (D14104)**.

Cohen, J., and J. Jones, 2011: Tropospheric precursors and stratospheric warmings. *J. Clim.*, **24**, 6562–6572.

Dai, Y., and B. Tan, 2016: The western pacific pattern precursor of major stratospheric sudden warmings and the ENSO modulation. *Env. Res. Lett.*, **11 (12)**, URL http://stacks.iop.org/1748-9326/11/i=12/a=124032.

Esler, J. G., and R. K. Scott, 2005: Excitation of transient rossby waves on the stratospheric polar vortex and the barotropic sudden warming. *J. Atmos. Sci.*, **62**, 3661–3682.

Garfinkel, C. I., A. Gordon, L. Oman, F. Li, S. Davis, and S. Pawson, 2017: Nonlinear response of tropical lower stratospheric temperature and water vapor to ENSO. *Atmos. Chem. Phys. Disc.*, Accepted.

Garfinkel, C. I., D. L. Hartmann, and F. Sassi, 2010: Tropospheric precursors of anomalous northern hemisphere stratospheric polar vortices. *J. Clim.*, **23**, 3282–3299.

Garfinkel, C. I., and C. Schwartz, 2017: MJO-related tropical convection anomalies lead to more accurate stratospheric vortex variability in subseasonal forecast models. *Geophys. Res. Lett.*, **44**, 10 054–10 062.

Garfinkel, C. I., D. W. Waugh, and L. M. Polvani, 2015: Recent hadley cell expansion: The role of internal atmospheric variability in reconciling modeled and observed trends. *Geophys. Res. Lett.*, **42**, 10 824–10 831.

Gerber, E. P., C. Orbe, and L. P. Polvani, 2009: Stratospheric influence on the tropospheric circulation revealed by idealized ensemble forecasts. *Geophys. Res. Lett.*, **36**.

Gerber, E. P., and Coauthors, 2010: Stratosphere-troposphere coupling and annular mode variability in chemistry-climate models. *J. Geophys. Res. Atmos.*, **115**.

Hitchcock, P., and P. H. Haynes, 2016: Stratospheric control of planetary waves. *Geophys. Res. Lett.*, **43**, 11 884–11 892.

Hitchcock, P., T. G. Shepherd, and G. L. Manney, 2013: Statistical characterization of arctic polar-night jet oscillation events. *J. Atmos. Sci.*, **26**, 20962116.

Hitchcock, P., and I. R. Simpson, 2014: The downward influence of stratospheric sudden warmings. *J. Atmos. Sci.*, **71**, 3856–3876.

Jucker, M., 2016: Are sudden stratospheric warmings generic? insights from an idealized gcm. *J. Atmos. Sci.*, **73**, 5061–5080.

Karpechko, A. Y., P. Hitchcock, D. H. W. Peters, and A. Schneidereit, 2017: Predictability of downward propagation of major sudden stratospheric warmings. *Q.J.R. Meteorol. Soc.*, **143**, 1459–1470.

Kidston, J., A. A. Scaife, S. C. Hardiman, D. M. Mitchell, N. Butchart, M. P. Baldwin, and L. J. Gray, 2015: Stratospheric influence on tropospheric jet streams, storm tracks and surface weather. *Nat. Geos.*, **8**, 433–440.

Kodera, K., H. Mukougawa, P. Maury, M. Ueda, and C. Claud, 2016: Absorbing and reflecting sudden stratospheric warming events and their relationship with tropospheric circulation. *J. Geophys. Res. Atmos.*, **121**, 80–94.

Lehtonen, I., and A. Y. Karpechko, 2016: Observed and modeled tropospheric cold anomalies associated with sudden stratospheric warmings. *J. Geophys. Res. Atmos.*, **121**, 1591–1610.

Limpasuvan, V., D. W. Thompson, and D. L. Hartmann, 2004: The life cycle of the northern hemisphere sudden stratospheric warmings. *J. Clim.*, **17**, 2584–2596.

Liu, C., K.-F. Tian, G. L. Manney, N. J. Livesey, Y. L. Yung, and D. E. Waliser, 2014: Northern hemisphere mid-winter vortex-displacement and vortex-split stratospheric sudden warmings: Influence of the Madden-Julian Oscillation and Quasi-Biennial Oscillation. *J. Geophys. Res. Atmos.*, **119**, 12,59912,620.

Marshall, A. G., and A. A. Scaife, 2010: Improved predictability of stratospheric sudden warming events in an atmospheric general circulation model with enhanced stratospheric resolution. *J. Geophys. Res.*, **115 (D16114)**.

Martineau, P., and S.-W. Son, 2013: Planetary-scale wave activity as a source of varying tropospheric response to stratospheric sudden warming events: A case study. *J. Geophys. Res. Atmos*, **118**, 10 994–11 006.

Martineau, P., and S.-W. Son, 2015: Onset of circulation anomalies during stratospheric vortex weakening events: The role of planetary-scale waves. *J. Clim.*, **28**, 7347–7370.

Martius, O., L. M. Polvani, and H. C. Davies, 2009: Blocking precursors to stratospheric sudden warming events. *Geophys. Res. Lett.*, **36 (L14806)**.

Matsuno, T., 1971: A dynamical model of the stratospheric sudden warming. *J. Atmos. Sci.*, **28**, 1479–1494.

Matthewman, N. J., J. G. Esler, A. J. Charlton-Perez, and L. M. Polvani, 2009: A new look at stratospheric sudden warmings. Part III: Polar vortex evolution and vertical structure. *J. Clim.*, **22**, 1566–1585.

Maycock, A. C., and P. Hitchcock, 2015: Do split and displacement sudden stratospheric warmings have different annular mode signatures? *Geophys. Res. Lett.*, **42**, 10 943–10 951.

Mitchell, D., L. J. Gray, J. A. Anstey, M. P. Baldwin, and A. J. Charlton-Perez, 2013: The influence of stratospheric vortex displacements and splits on surface climate. *J. Clim.*, **26**, 2668–2682.

Molod, A., M. Takacs, M. Suarez, J. Bacmeister, I.-S. Song, and A. Eichmann, 2012: The geos-5 atmospheric general circulation model: Mean climate and development from merra to fortuna: Tech. rep. ser. on global model. and data assimilation. Tech. rep., Nat. Aeronautics and Space Admin., Goddard Space Flight Cent., Greenbelt, Md.

Nakagawa, K. I., and K. Yamazaki, 2006: What kind of stratospheric sudden warming propagates to the troposphere? *Geophys. Res. Lett.*, **33 (L04801)**.

Nishii, K., H. Nakamura, and Y. Orsolini, 2010: Cooling of the wintertime arctic stratosphere induced by the western pacific teleconnection pattern. *Geophys. Res. Lett.*, **37 (L13805)**.

O'Callaghan, A., M. Joshi, D. Stevens, and D. Mitchell, 2014: The effects of different sudden stratospheric warming types on the ocean. *Geophys. Res. Lett.*, **41**, 7739–7745.

Pawson, S., R. S. Stolarski, A. R. Douglass, P. A. Newman, J. E. Nielsen, S. M. Frith, and M. L. Gupta, 2008: Earth observing system chemistry-climate model simulations of stratospheric ozone-temperature coupling between 1950 and 2005. *J. Geophys. Res. Atmos*, **113 (D12103)**.

Plumb, R. A., 1985: On the three-dimensional propagation of stationary waves. *J. Atmos. Sci.*, **42**, 217–229.

Polvani, L. M., and P. Kushner, 2002: Tropospheric response to stratospheric perturbations in a relatively simple general circulation model. *Geophys. Res. Lett.*, **29 (7)**.

Polvani, L. M., and D. W. Waugh, 2004: Upward wave activity flux as a precursor to extreme stratospheric events and subsequent anomalous surface weather regimes. *J. Clim.*, **17 (18)**, 3548–3554.

Rienecker, M. M., and Coauthors, 2008: The GEOS-5 data assimilation system documentation of versions 5.0.1, 5.1.0, and 5.2.0. *Technical Report Series on Global Modeling and Data Assimilation*, **27**, 347–367.

Runde, T., M. Dameris, H. Garny, and D. E. Kinnison, 2016: Classification of stratospheric extreme events according to their downward propagation to the troposphere. *Geophys. Res. Lett.*, **43**, 6665–6672.

Scaife, A. A., and Coauthors, 2012: Climate change projections and stratosphere-troposphere interaction. *Clim. Dyn.*, **38**, 2089–2097.

Seviour, W. J. M., L. J. Gray, and D. M. Mitchell, 2016: Stratospheric polar vortex splits and displacements in the high-top CMIP5 climate models. *J. Geophys. Res. Atmos.*, **121**, 1400–1413.

Seviour, W. J. M., D. M. Mitchell, and L. J. Gray, 2013: A practical method to identify displaced and split stratospheric polar vortex events. *Geophys. Res. Lett.*, **40**, 5268–5273.

Sigmond, M., J. F. Scinocca, V. V. Kharin, and T. G. Shepherd, 2013: Enhanced seasonal forecast skill following stratospheric sudden warmings. *Nat. Geosci.*, **6**, 98–102.

Sjoberg, J. P., and T. Birner, 2012: Transient tropospheric forcing of sudden stratospheric warmings. *J. Atmos. Sci.*, **69**, 3420–3432.

Smith, D., A. A. Scaife, and B. Kirtman, 2012: What is the current state of scientific knowledge with regard to seasonal and decadal forecasting? *Env. Res. Lett.*, **7 (015602)**.

Thompson, D. W. J., M. P. Baldwin, and J. M. Wallace, 2002: Stratospheric connection to northern hemisphere wintertime weather: Implications for prediction. *J. Climate.*, **15**, 1421–1428.

Tomassini, L., E. P. Gerber, M. P. Baldwin, F. Bunzel, and M. J. Giorgetta, 2012: The role of stratosphere-troposphere coupling in the occurrence of extreme winter cold spells over northern europe. *J. Adv. Model. Earth Syst.*, **4**.

Tripathi, O. P., and Coauthors, 2014: The predictability of the extratropical stratosphere on monthly time-scales and its impact on the skill of tropospheric forecasts. *Q. J. R. Meteorol. Soc.*, **141**, 987–1003.

LIST OF TABLES

Karpechko et al. (2017)						
Method	*Total*		*DW*		*NDW*	
Charlton and Polvani (2007) Wind Reversal	962		506		456	
	Splits	*Displacements*	*Splits*	*Displacements*	*Splits*	*Displacements*
Seviour et al. (2013) 2-D Moments	400	500	191	280	209	220
Runde et al. (2016)						
Method	*Total*		*DW*		*NDW*	
Charlton and Polvani (2007) Wind Reversal	962		418		544	
	Splits	*Displacements*	*Splits*	*Displacements*	*Splits*	*Displacements*
Seviour et al. (2013) 2-D Moments	400	500	148	239	252	261
Jucker (2016) – Absolute Criterion						
Method	*Total*		*DW*		*NDW*	
Charlton and Polvani (2007) Wind Reversal	962		370		592	
	Splits	*Displacements*	*Splits*	*Displacements*	*Splits*	*Displacements*
Seviour et al. (2013) 2-D Moments	400	500	135	190	265	310
Jucker (2016) – Relative Criterion						
Method	*Total*		*DW*		*NDW*	
Charlton and Polvani (2007) Wind Reversal	962		536		426	
	Splits	*Displacements*	*Splits*	*Displacements*	*Splits*	*Displacements*
Seviour et al. (2013) 2-D Moments	400	500	187	288	213	212

TABLE 1. Table showing the number of SSWs according to the two main SSW definitions used in this study; the wind reversal criterion at 60°N, 10 hPa (Charlton and Polvani 2007), and the 2-D vortex moments to identify split and displacement events (Seviour et al. 2013). Also included are the total number of DW and NDW SSW events calculated using the definitions of Karpechko et al. (2017), Runde et al. (2016), and the absolute-criterion and relative-criterion definitions of Jucker (2016). See text for further details.

LIST OF FIGURES

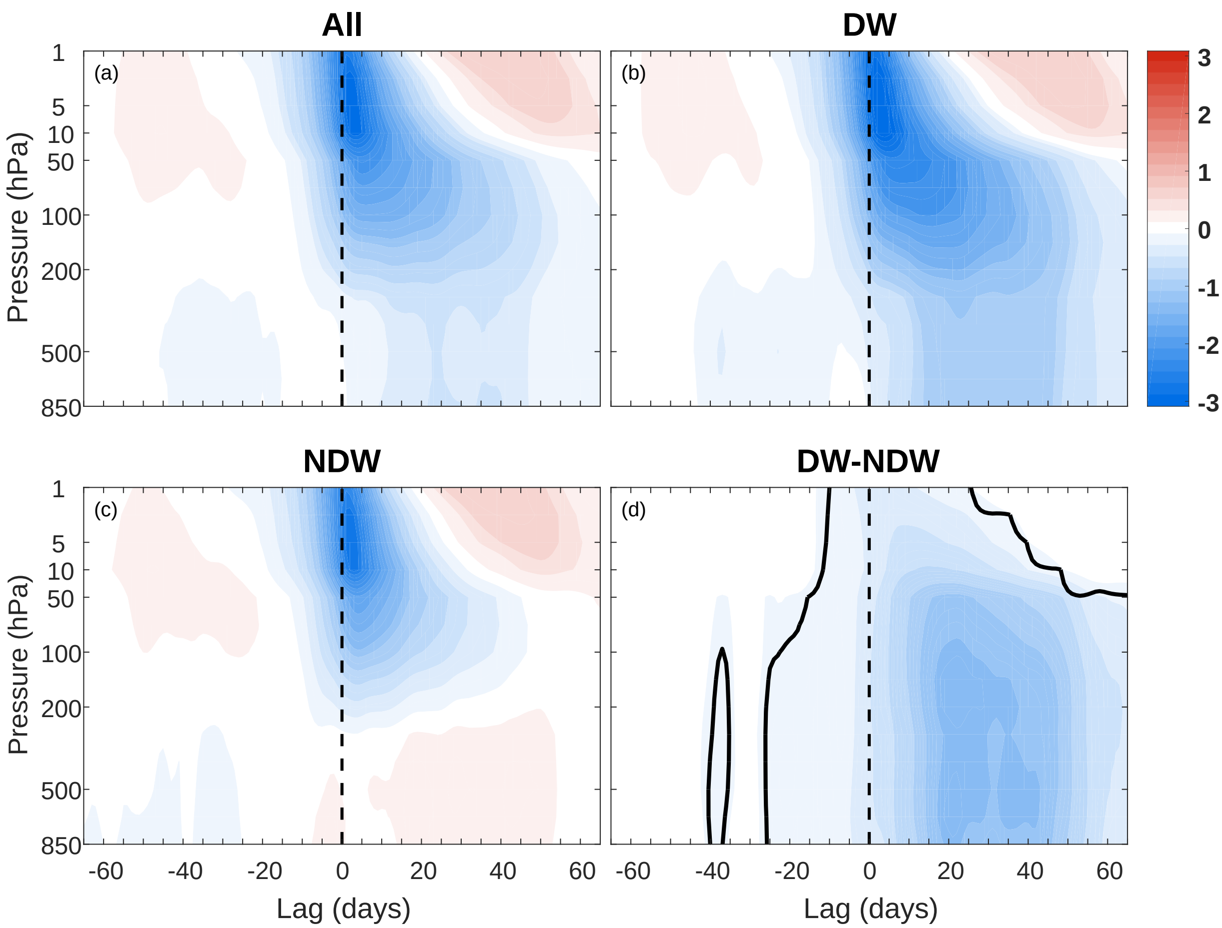

FIG. 1. The composite evolution of the NAM index for (a) all SSWs calculated in the entire ensemble of integrations; (b) DW-propagating SSWs calculated using the Karpechko et al. (2017) criteria (see section c); (c) same as (b) except for NDW-propagating SSW events; and (d) the composite difference between the DW- and NDW-propagating events (DW-NDW). The units are in standard deviations. The thick black line in (d) represents statistical significance at the 95% level.

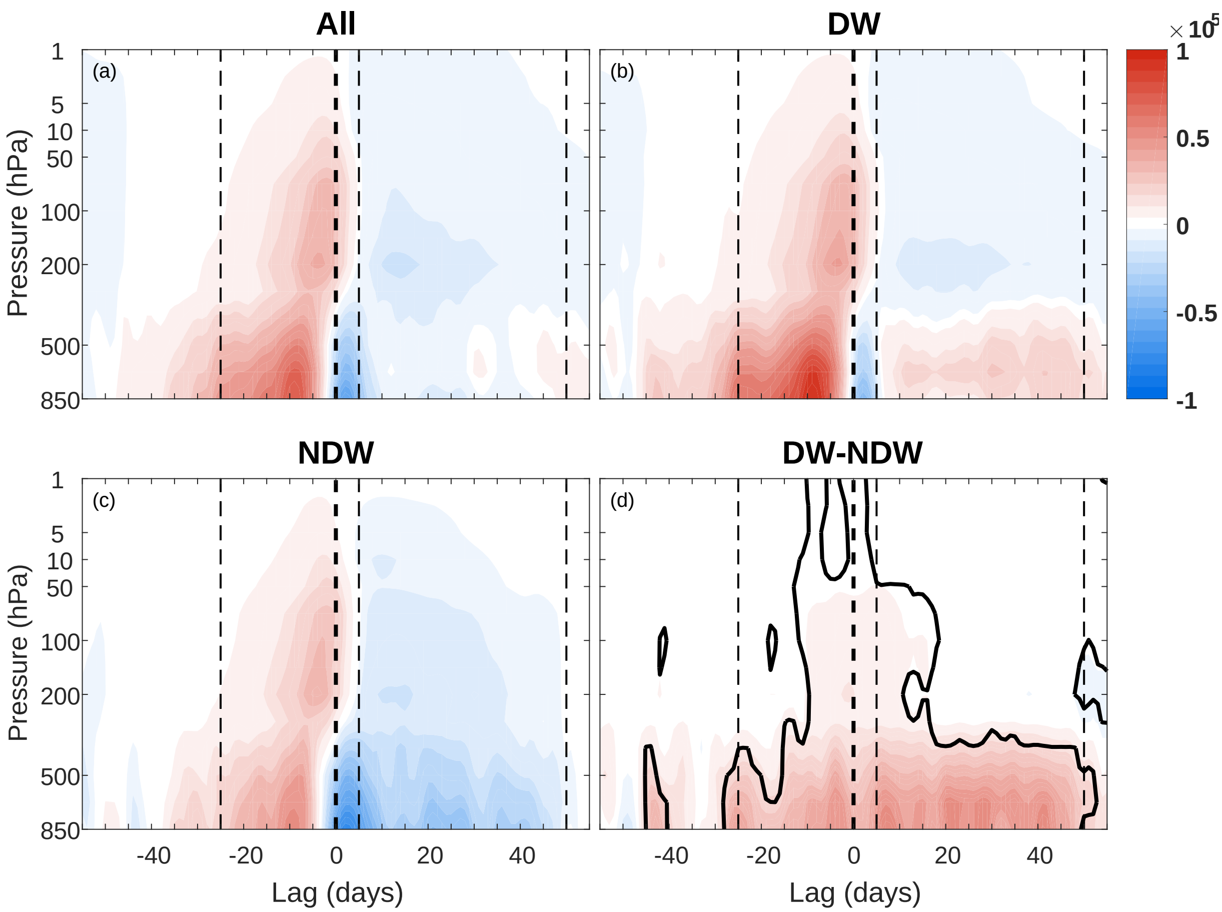

FIG. 2. Same as figure 1 except for the anomalous vertical component of the Eliassen-Palm flux, $F^{(z)}$ (see text), averaged over the latitude band of 45-75°N and filtered for planetary waves 1 and 2. $F^{(z)}$ has units of kg s^{-2}. The dashed vertical lines represent the start and end of the different lag stages used throughout the remainder of the manuscript (see text). The dashed line corresponding to zero lag has a double thickness for clarity.

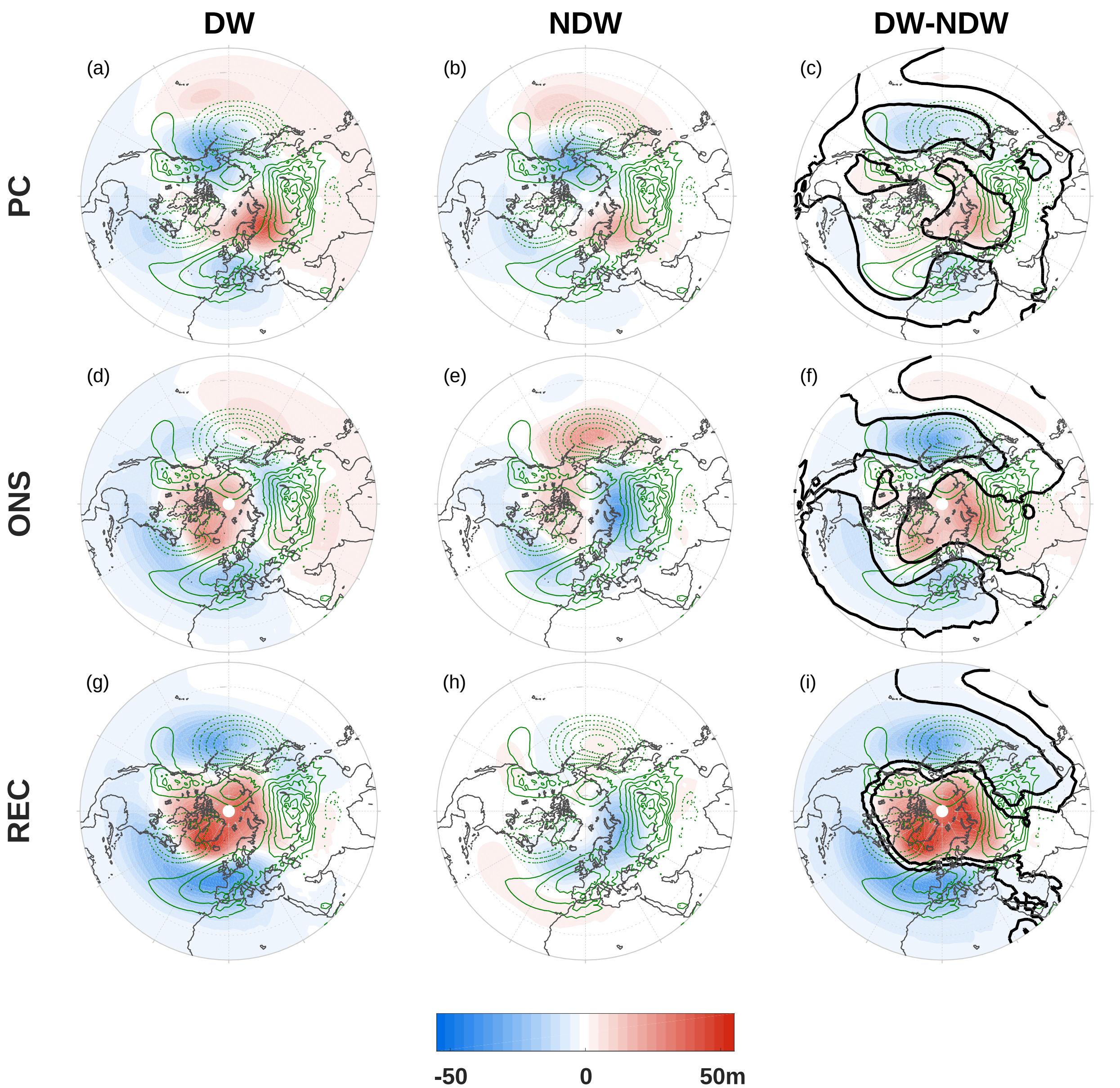

FIG. 3. Geopotential height Z anomalies (shading; units m) at 850 hPa, averaged over the (top row) PC stage, (middle row) ONS stage and (bottom row) REC stage, and composited over: (left column) DW events; (middle column) NDW events; (right column) DW-NDW differences. Green contours show the Nov-Feb climatology calculated as the average over all of the 40 experiments with a contour interval of 15 m. The thick black line is as in figure 1.

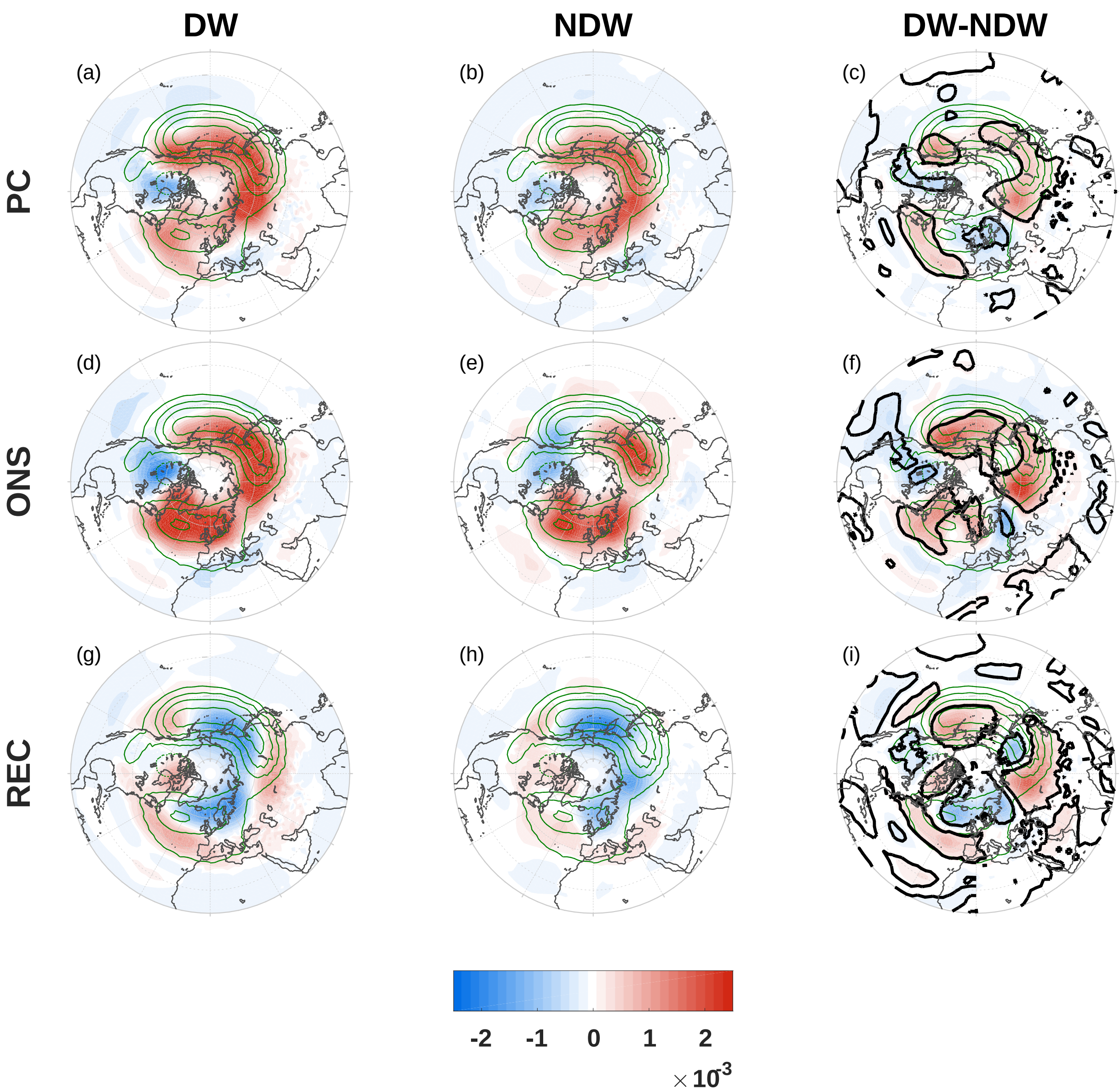

FIG. 4. Same as figure 3, except for the anomalous vertical component of the Plumb flux ($F_p^{(z)}$; see text) at 150 hPa. Green contours represent the climatology with a contour interval of 0.002 m^2 s^{-2}.

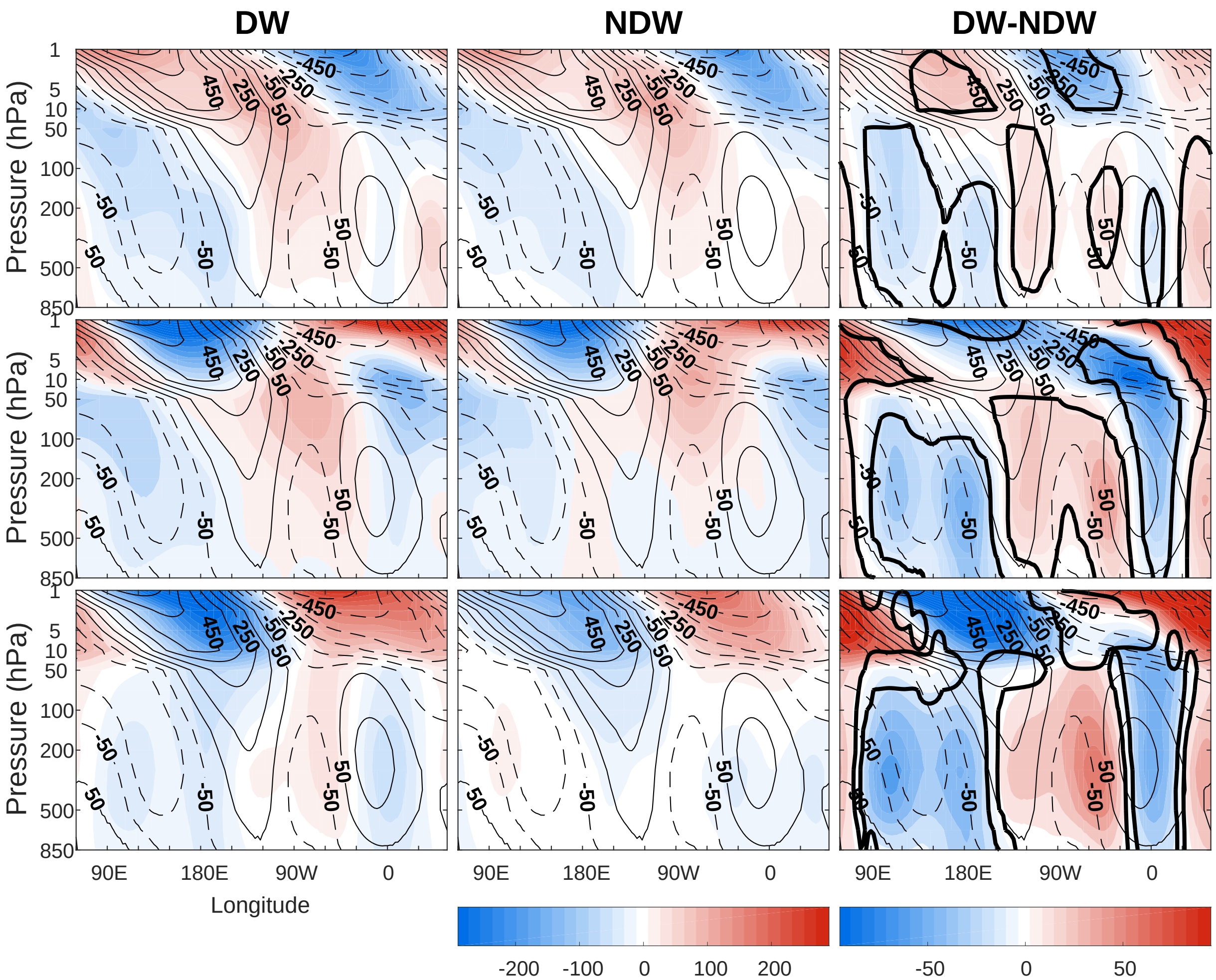

FIG. 5. Same as figure 3 except for the longitude-height cross-sections of Z' (i.e., deviation from the zonal-mean) averaged over the latitude band 50-60°N. The units are in *m*. Thin black contours show the Nov-Feb climatology calculated as the average over all of the 40 experiments with contours at -650,-550,...,550,650 m.

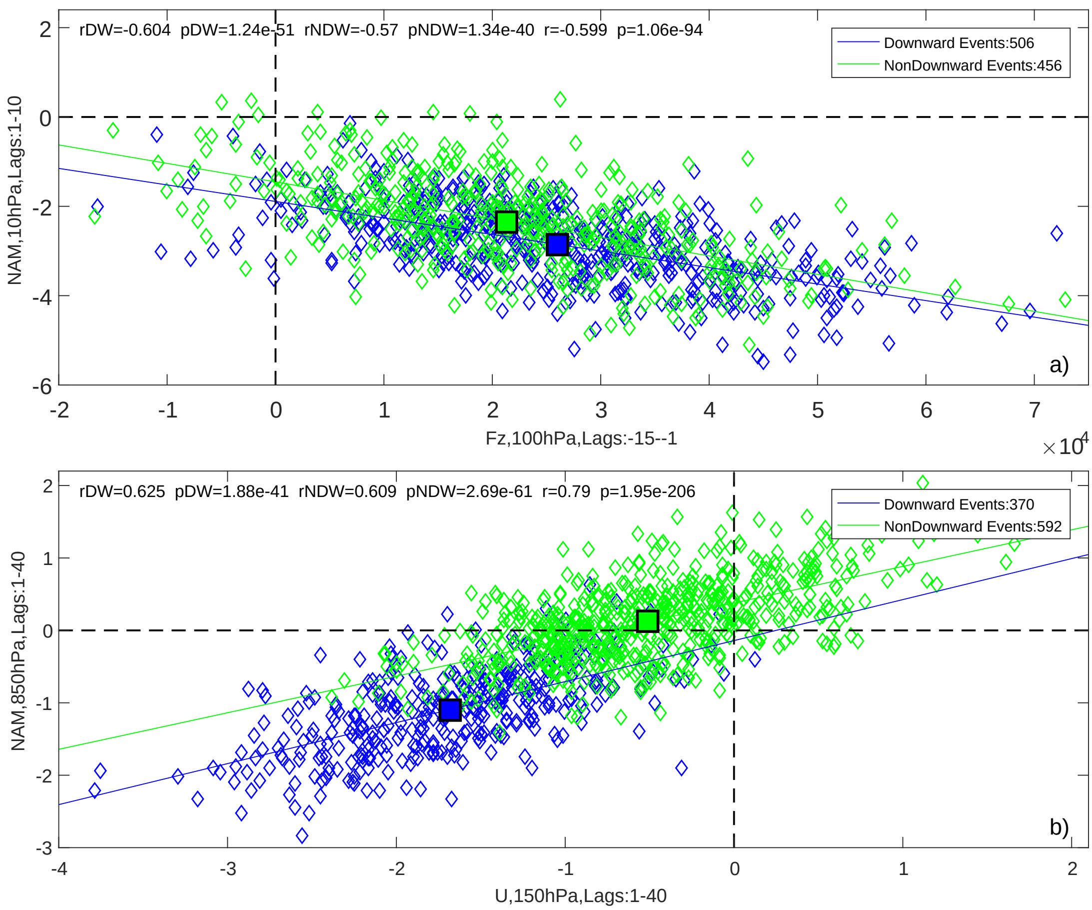

FIG. 6. Scatter plots of (a) the EP flux $F^{(z)}$ at 100 hPa averaged over lags -15 to -1, against the NAM index at 10 hPa averaged over lags +1 to +10, and (b) $\overline{u}$ at 150 hPa and averaged over 50-80°N and lags +1 to +40 against the NAM index at 850 hPa averaged over lags +1 to +40. Blue (green) diamonds, lines and squares represent, respectively, individual DW (NDW) SSW events, the corresponding lines of best fit, and the overall composite averages. The rDW (pDW), rNDW (pNDW) and r (p) represent the correlation coefficients and p-values for the DW events, NDW events, and total, respectively. In (a), the R^2 value for the DW and NDW events are 0.36 and 0.32, and in (b), the R^2 values are 0.39 and 0.37. Note that the DW and NDW events in (a) have been determined using the Karpechko et al. (2017) definition, whereas in (b) they are calculated using the absolute-criterion definition of Jucker (2016).

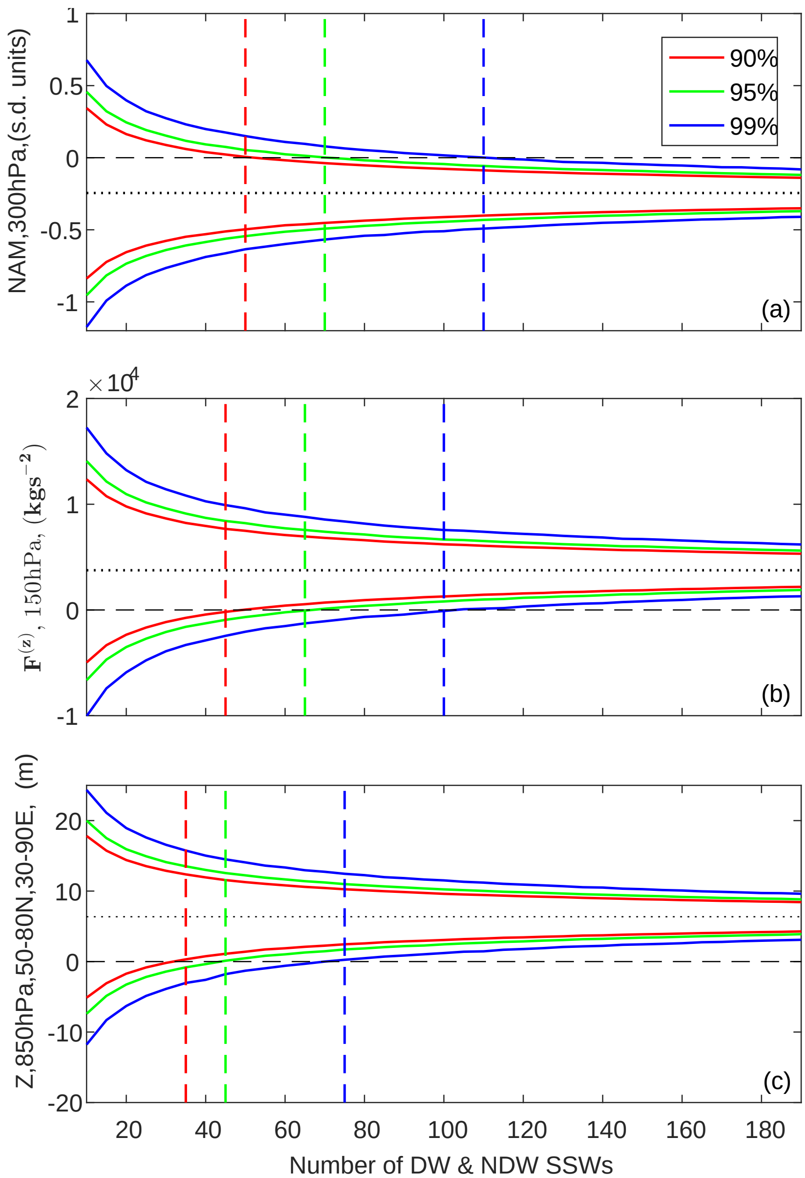

FIG. 7. Confidence intervals for the difference (DW-NDW) of (a) the NAM index averaged over lags -25 to -1 and at 300 hPa, (b) $F^{(z)}$ anomalies filtered for waves 1-2 and area-averaged over 45-75°N, and (c) Z anomalies at 850 hPa averaged over 50-80°N, 30-90°E and over lags -25 to -1. The confidence intervals are estimated using a Monte Carlo simulation of 100,000 repetitions for different sample sizes ranging from 10 to 455. The red, green and blue curves represent the 90%, 95% and 99% confidence intervals, and the respective coloured vertical dotted lines represent the sample size for which the upper bound crosses zero (indicated by the dashed black line). The dotted black line represents the overall DW-NDW composite over all DW and NDW events, as shown in figures 1- 3, respectively.

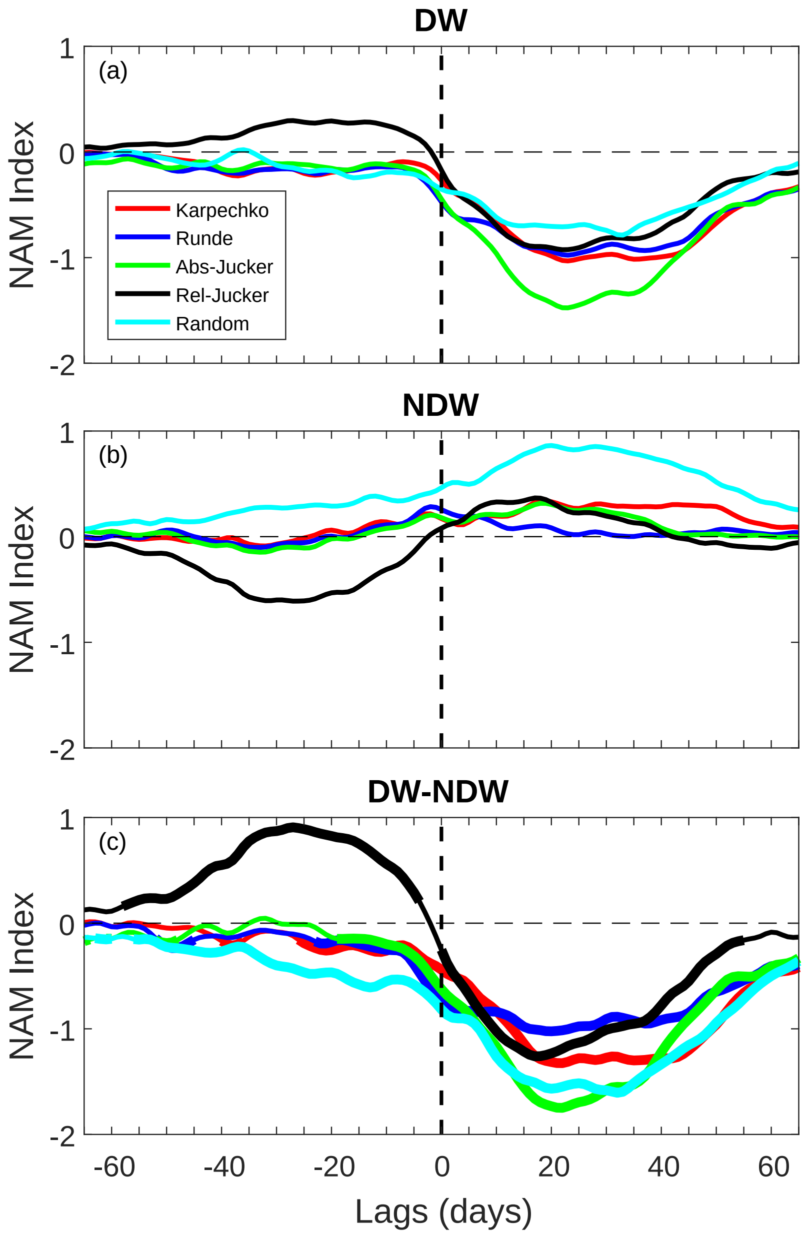

FIG. 8. NAM index at 500 hPa composited over (a) DW events, (b) NDW events, and (c) DW-NDW differences, for the four DW definitions introduced in section 2 c: red, dark blue, green and black lines represent the NAM index for the Karpechko et al. (2017) definition, Runde et al. (2016) definition, and absolute- and relative-criterion definitions of Jucker (2016), respectively. There is also an additional cyan line representing the NAM index found using a random selection of tropospheric NAM events (see text). The thick lines represent statistical significance at the 95% level.

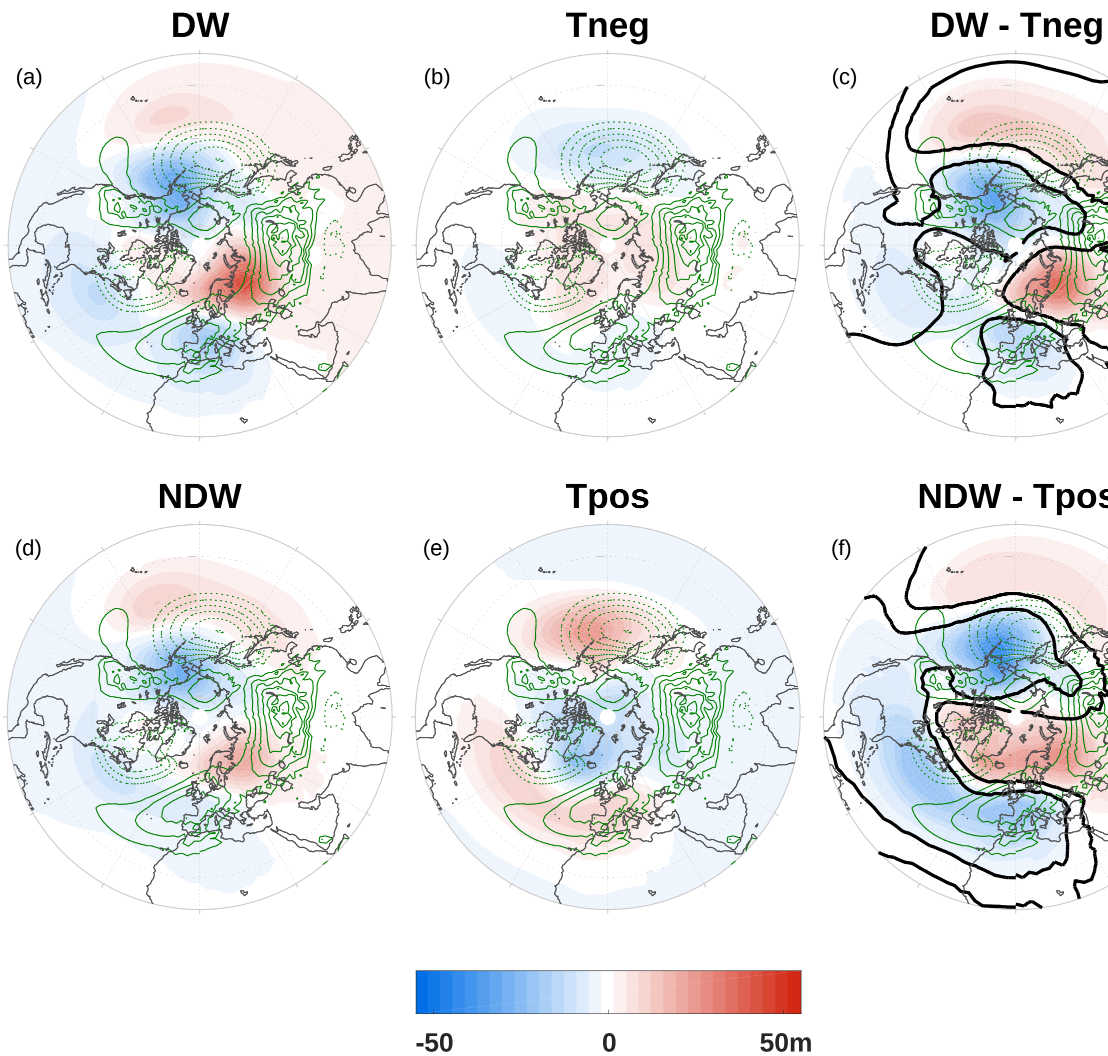

1081 FIG. 9. Z anomalies at 850 hPa averaged over the PC stage (lags -25 to -5) for the (a) DW SSWs composite,
1082 (b) Tneg events composite, (c) DW-Tneg difference, (d) NDW SSWs composite, (e) Tpos events composite, and
1083 (f) NDW-Tpos difference. See figure 3 for details on the shading and different contours. Note that panels (a)
1084 and (d) are repeated from panels (a) and (b) in figure 3.

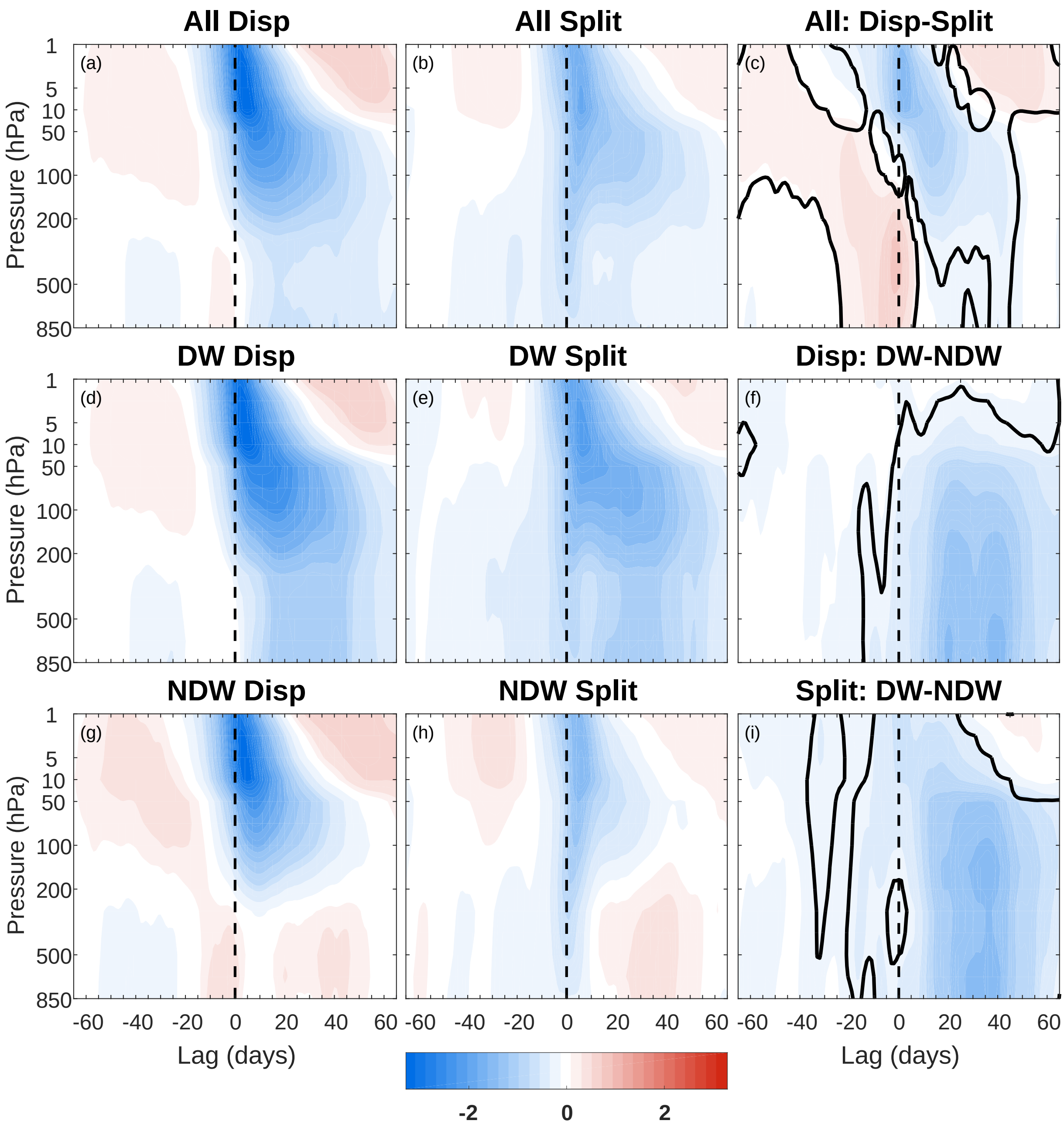

FIG. 10. Composite evolution of the NAM index divided into displacements (left column) and splits (middle column) and subdivided further into the total (top row), DW-propagating (middle row) and NDW-propagating (bottom row). The right column shows the Disp-Split (top), DW-NDW displacements (middle), and DW-NDW splits (DW-NDW). See figure 1 for further details on shading and different contours.

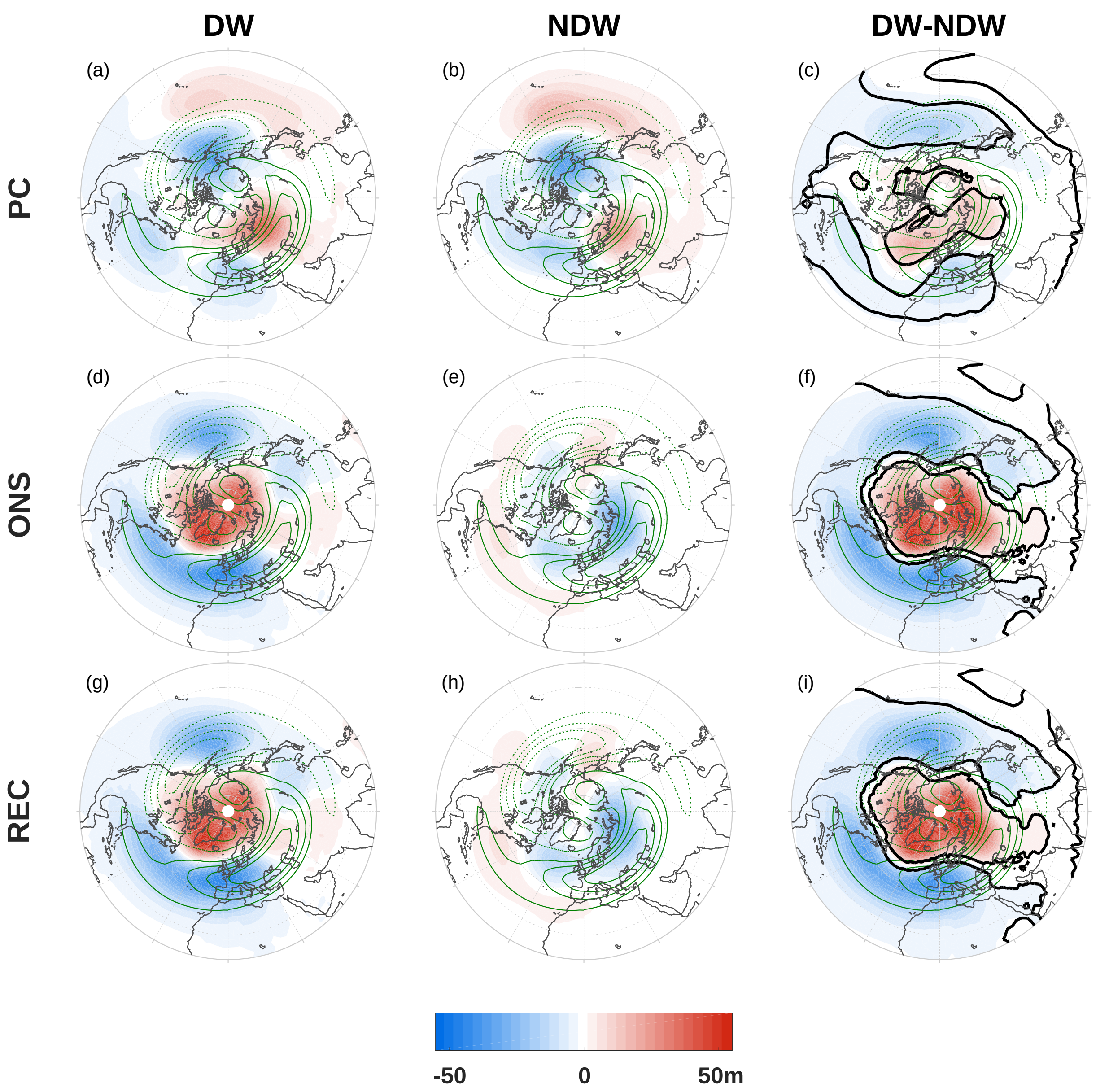

FIG. 11. As in figure 3, except for Z at 850 hPa for the displacement SSWs. Note that the green contours show the climatological Z filtered only for wave-1 and with a contour interval of 10 m.

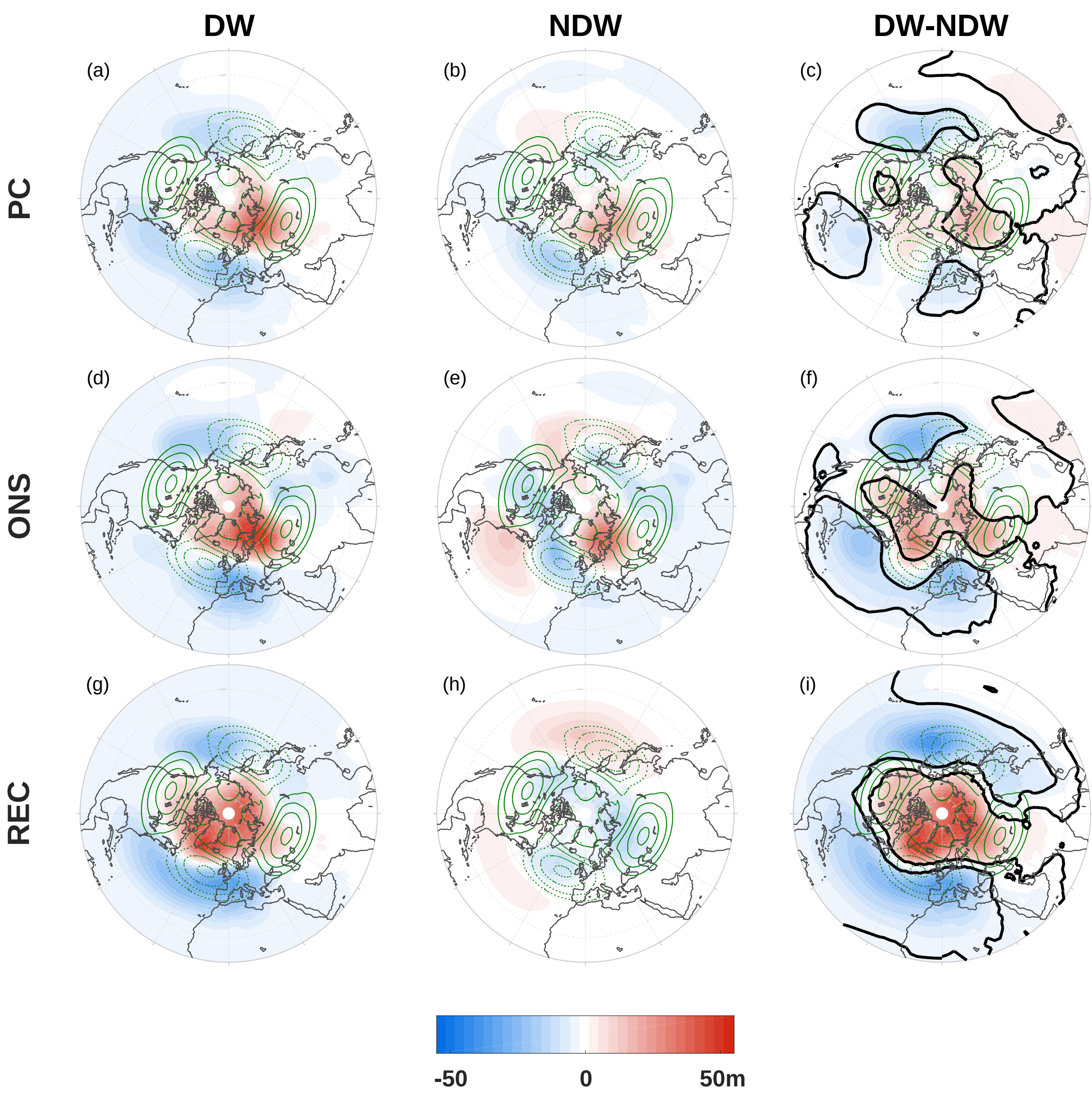

1091 FIG. 12. As in figure 3, except for split SSWs, and the green contours showing the climatological Z' filtered
1092 only for wave-2 and with a contour interval of 10 m.

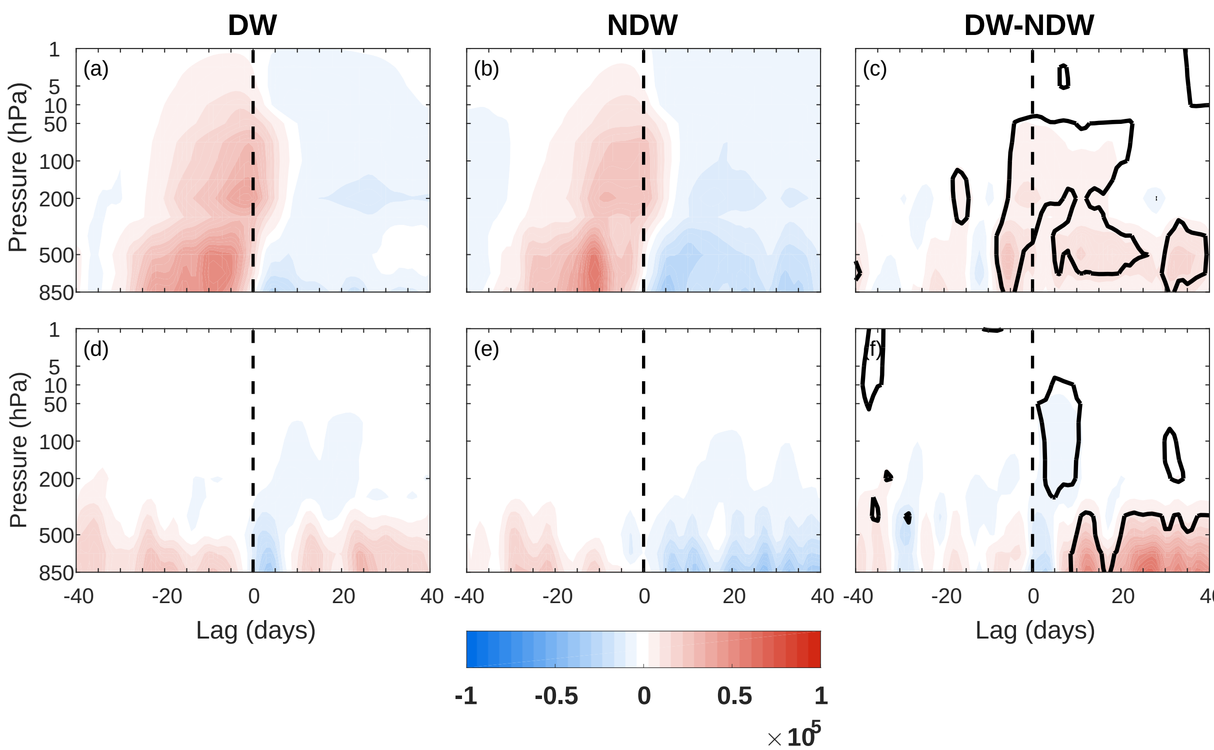

FIG. 13. Height-time plot of F_z averaged over 45-75°N, for the displacement SSWs composited over (left column) DW events, (middle) NDW events and (right) DW-NDW difference. Top row shows F_z for wave-1 and bottom row shows F_z for wave-2. Thick black contour in the difference plots represent statistical significance at the 95% level.

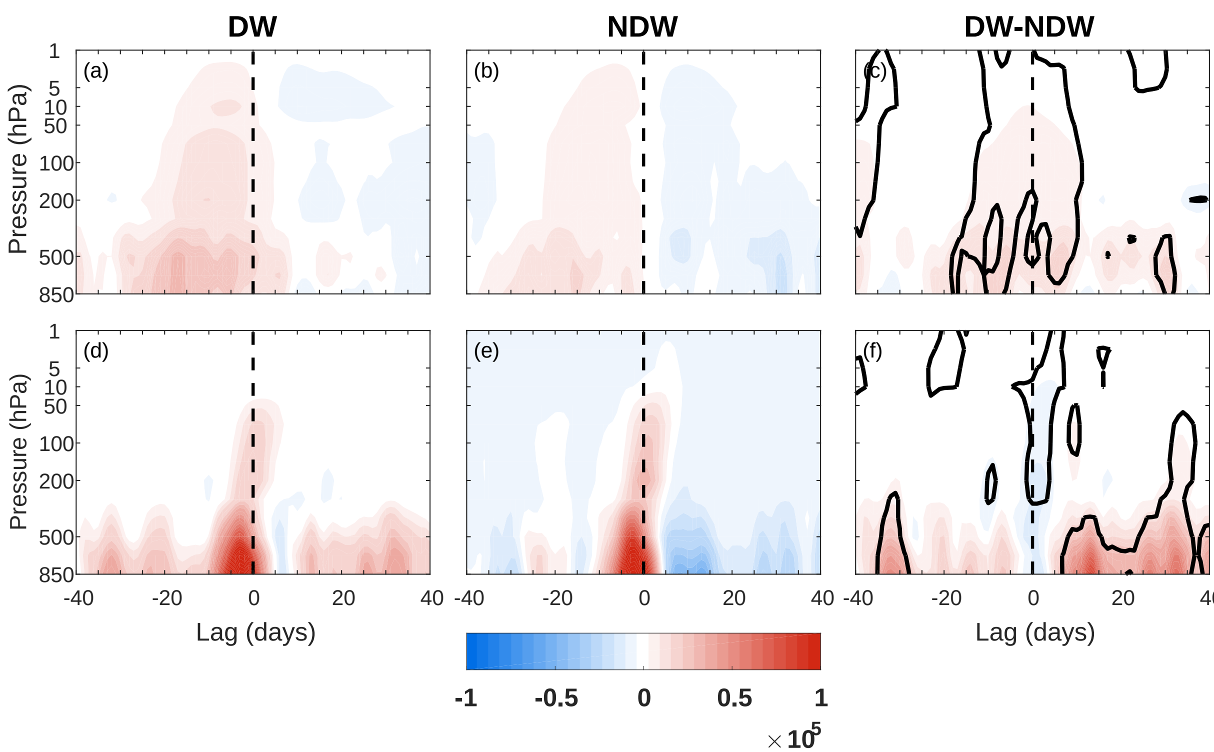

FIG. 14. As in figure 13, except for split SSWs.